



Volume IV

Appendix F.2

Follow the TPS

This Appendix presents an analysis to confirm or refute the following hypothesis put forth by the Columbia Accident Investigation Board during the launch of STS-107 Mission: A briefcase-sized piece of External Tank foam struck the RCC left wing leading edge system, compromising the RCC. During entry, the damage to the RCC led to structural failure of the wing, the tragic loss of Columbia, and the STS-107 crew.

THIS PAGE INTENTIONALLY LEFT BLANK

“Follow the TPS”: An Analysis of What Occurred to the Thermal Protection System (TPS) During the Flight of Shuttle Columbia on STS 107

J. O. Arnold [†], H. E. Goldstein [‡], and D. J. Rigali ^λ

Executive Summary

This appendix presents an analysis to confirm or refute the following hypothesis put forth by the Columbia Accident Investigation Board (CAIB): During launch of the Space Transportation System (STS) 107 Mission, a briefcase-sized piece of External Tank (ET) foam struck the Reinforced Carbon-Carbon Left Wing Leading Edge Subsystem (RCC LW LESS), compromising the RCC. During entry, the damage to the RCC led to structural failure of the wing, the tragic loss of Columbia and the STS 107 crew.

The focus of this analysis was on what happened to the Thermal Protection System (TPS). The analysis supports the hypothesis and identifies the probable location of the breach. The analysis assumed that the ET foam strike was the initiating event. Other investigators have shown by test and analysis that the foam strike could have caused a breach in the RCC. Comparison of events following from the hypothesis to observations from flight data, debris forensics, ground test and analysis strongly suggests that the breach was in the lower part of RCC Panel 8, and that it existed at entry interface (EI).

Key information, in temporal order, from flight observations include: **Ascent, post foam strike:** Modular Auxiliary Data System/Orbiter Experiments (MADS/OEX) data from a thermocouple mounted behind the leading edge wing spar, behind Panel 9, recorded off-nominal temperature increases during ascent. **Entry:** MADS/OEX data from four sensors show the progression of damage is from the RCC toward the aft of the vehicle. Later, the thermocouple on the spar, behind Panel 9, recorded an abrupt temperature increase at Entry Interface + 487 seconds, interpreted to be caused by superheated air penetrating the leading edge wing spar. Analysis by NASA shows that these observations can be accounted for by the presence of a hole, 6 -> 10 inches in diameter, in the lower portion of RCC Panel 8. Greater than normal temperatures subsequently measured on the Orbital Maneuvering Systems (OMS) pod correlates with ground based observations of debris leaving Columbia. Later, a photograph was taken from the Starfire facility at Kirtland Air Force Base showing left wing damage consistent with the hypothesis.

Compelling evidence to support the hypothesis comes from the debris from Columbia. Study of the debris revealed significant damage in the LW RCC Panel 8/9 area. This included ablation, or “sharpening” of the very durable RCC and melting of high temperature metal fixtures and insulation, internal to the WLESS, believed to be caused by prolonged exposure to a superheated airflow. Arc jet simulations of RCC in such a superheated air stream support this conclusion. Flow out of a slot in the lower juncture between LW RCC Panels 8 and 9 caused severe erosion and flow patterning on the carrier panels below RCC Panel 9. Chemical analysis of “slag” on the debris shows “layering” that correlates with the hypothesis.

The authors believe it is quite likely that the breach caused by the foam strike was a hole of at least 6 -> 10 inches in diameter in the lower part of RCC Panel 8. Finally, it is noted that it is unreasonable to assign blame to the TPS for the tragic accident of Columbia. The total TPS for the shuttle has performed admirably during all of the STS flights (including STS 107) in the environments for which it was designed. Upgrades to the TPS being planned will make it better. The primary technical issue for the STS 107 accident is the integrity of the ET foam during launch.

[†] Senior Scientist, University of California, Santa Cruz and Retired Chief, Space Technology Division, NASA Ames Research Center and Fellow, AIAA.

[‡]Consultant, Valador, Consultant, Research Institute for Advanced Computer Science (RIACS), Retired Chief Scientist, Space Technology Division and Retired, Chief, Thermal Protection Systems Branch, NASA Ames Research Center and Fellow, AIAA.

^λConsultant, Valador, Retired Director of Aerospace Systems Development Center, Sandia National Laboratory.

Introduction

A hypothesis, presented by the Columbia Accident Investigation Board (CAIB) chair, Admiral H. Gehman, is that the tragic loss of the crew of STS 107 and the Space Shuttle Columbia was caused by a briefcase-sized piece of External Tank (ET) foam insulation striking the leading edge of Columbia's left wing (LW) about 82 seconds after the lift off of Space Transportation Systems (STS) 107 mission. The hypothesis assumes this strike compromised the thermo-structural wing leading edge made of reinforced carbon-carbon (RCC). During re-entry on February 1, 2003, superheated air entered a breach in the wing leading edge subsystem (WLESS), eventually leading to structural failure of the wing, break-up of the vehicle and loss of the crew.

Soon after the CAIB investigation began, board member G. Scott Hubbard assigned the authors of this appendix to "Follow the Thermal Protection System (TPS)" to develop supporting and/or refuting evidence for the aforementioned hypothesis (among others). Within the context of the charter of CAIB Group 3, the assignment was to look exclusively at "what happened to the TPS" during the flight, while those from other groups focused on issues such as aging or maintenance problems of the TPS that might have been the root cause of the problem.

Detailed analysis by NASA (References 1 and 2) of the launch imagery and comprehensive Computational Fluid Dynamics (CFD) simulations indicate that the area struck by the ET foam was on the LW LESS in the lower RCC Panel 5-8 areas. Tests (Reference 3) at Southwest Research Institute have been conducted where projectiles of ET foam (mass on the order of 1.7 pounds, sizes the order of a briefcase) were fired at speeds of around 770 ft/sec, impacting full-scale wing leading edge components to assess how much damage such a strike could inflict. These tests were designed with the help of newly developed physics-based codes, which were also used to interpret the results. These results show that such an impact does cause severe damage to the RCC. Observed damage included cracking and displacements of the panels and seals between them (T-Seals), as well as the formation of holes as large as 16 inches by 16 inches.

Furthermore, important data obtained during the flight of STS 107 from the Modular Auxiliary Data System (MADS)/Orbiter Experiments (OEX) were secured through the recovery of a magnetic tape in the Columbia debris. This information (Reference 4) has provided important facts regarding the sequence of events occurring during the STS 107 entry. Only the key MADS/OEX data establishing the temporal evolution of heating events is discussed herein.

Recovered debris from Columbia revealed significant damage in the RCC Panel 8/9 area. This included heavy ablation, or "sharpening" of the very durable RCC, and melting of metal fixtures and insulation, internal to the WLESS. Significant melting of LESS RCC mounting hardware is observed only in the Panel 8/9 area of the left wing. This debris evidence is believed to have occurred during exposure to a superheated flow environment, internal to the LW LESS, lasting for hundreds of seconds. Arc jet simulations (References 5, 6 and 7) of RCC in such a superheated air stream support this conclusion.

In the sections that follow, the timeline of events, analysis of key OEX data, aerothermodynamics/thermal analysis and debris forensics are compared to the hypothesis. The preponderance of evidence leads to the conclusion that the aforementioned hypothesis is what truly happened: An ET foam strike during launch created a breach in the LW LESS in the area of the lower RCC Panel 8. The breach was present at the Entry Interface (EI). Superheated air was ingested into the WLESS, melted through the leading edge spar, introduced hot gas into the wing box, weakened the structure and led to the loss of Columbia and the STS 107 crew.

Normal Entry Environment

In order to understand the function and need for the Shuttle's TPS, a brief review of the Shuttle reentry environment is discussed herein. Figure 1, supplied by NASA, shows two important aspects of the expected STS 107 entry profile: geodetic altitude versus Greenwich Mean Time (GMT) and normalized entry heating versus GMT. Entry was defined to begin at an altitude of 400,000 ft at GMT 13 hours, 44 minutes and 09 seconds (13:44:09). As can be seen from Figure 1(a), the time to descend from EI to 200,000 ft is approximately 15 minutes. During this period, Columbia passed over the coast of California, heading for an expected landing at the Kennedy Space Center (KSC), executing one roll to the right and one roll to the left during descent. Columbia entered as expected at a nominal angle of attack of 40 degrees, with its black underbelly facing into the wind. This maneuver and the rather blunt nose cap and wing leading edges of the Shuttle have the effect of reducing aeroconvective heating (blunt body concept, Reference 8).

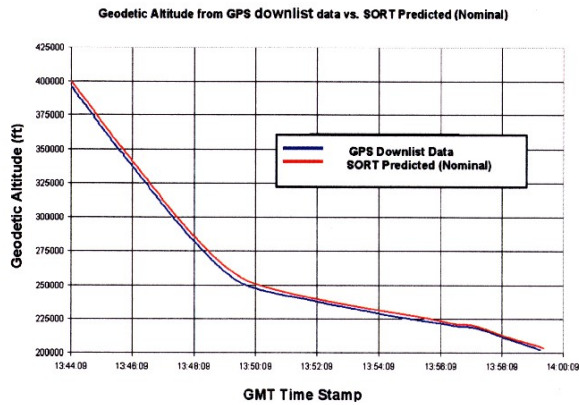


Figure 1(a): Normal Entry: Geodetic Altitude vs. GMT. Entry Interface (EI) at 400,000 ft. Angle of Attack: 40 Degrees.

Figure 1(b) shows a plot of expected heating rates, normalized to the stagnation point near the nose of the vehicle versus GMT. Here, one can see that the heating rate is nearly constant at a maximum for about 9 minutes. The heating rate on the landing gear door area in the wing is considerably lower than that at the nose of the vehicle. Color-coding on the figure shows TPS surface temperatures caused by these heating rates.

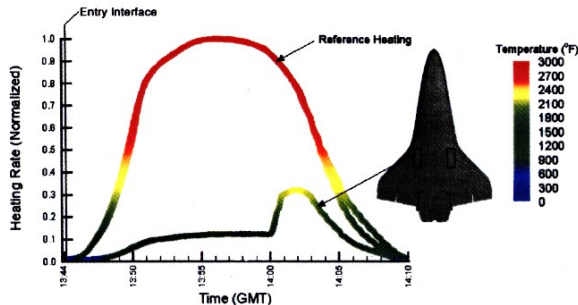


Figure 1(b): Normal Entry: Normalized Heating Rates vs. GMT. Entry Interface (EI) at Altitude: 400,000 ft, Angle of Attack: 40 Degrees.

Figure 2, based on Computational Fluid Dynamics (CFD) (Courtesy of NASA JSC J. Caram/NASA Ames J. Brown and D. Prabhu) gives one a feel for the vehicle environment experienced and flow field about the Space Shuttle during a “nominal entry”, i.e., no damage to the vehicle. These results are state-of-the-art real-gas CFD, Reynolds Averaged Navier-Stokes solutions, assuming a laminar boundary layer. Real-gas effects include chemically reacting flows among the constituents; N_2 , O_2 , NO, N and O. At these conditions, there is nearly complete dissociation of diatomic oxygen (O_2) and

formation of NO. A very slight amount of ionization occurs in reality. This is not accounted for in the solutions, but this has little effect on entry heating. TPS response is accounted for including realistic wall catalytic effects and surface emissivity. Shuttle surfaces tend to be non-catalytic, meaning that the atomic oxygen and nitrogen in the boundary layer do not recombine, reducing the sensible heat into the TPS. Full detail of the code used for this work and its validation against ground and flight (Shuttle) data can be found in Reference 9. The code used, GASP (commercially available by Aerosoft, Inc), is one of several codes used by NASA in the analysis of the Columbia accident. Results from other codes, including LAURA (Reference 10), developed by NASA Langley, will be discussed later.

Figure 2(a) shows temperature contours within the shock layer that forms about the Space Shuttle during entry. Flow is from lower left to upper right. A view in the pitch plane at the centerline of the vehicle is shown for conditions at 227,424 ft and an angle of attack of 39.59 degrees. The outer, blue envelope representing free stream or ambient air is outside of the shock front, within the computational grid. The rapid change in color represents the shock front. One can see that gas temperatures in the forebody, nose region of the shock layer, behind the shock front exceed 20,000 °F (red -> magenta). As the gases expand in the shock layer, cooling occurs, and the forebody gas temperatures drop into the area of 12,000 -> 9000 °F (yellow -> green) along the windward side or underbelly of the vehicle. In the leeward portion of the flow, gas temperatures are much cooler (4,000 - 2,000 °F) as shown by the blue-green color.

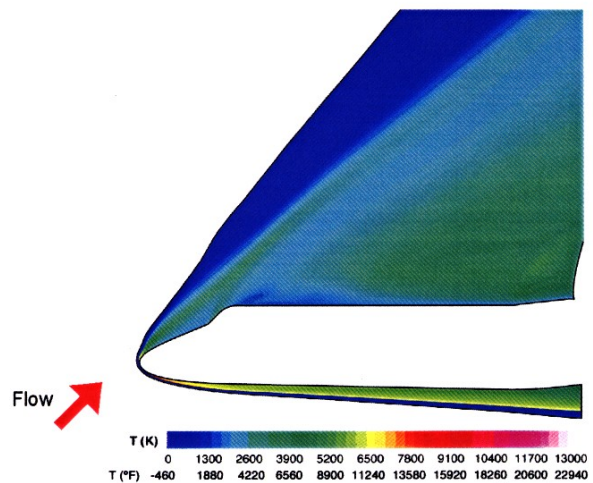


Figure 2 (a): Gas Temperatures from CFD Solution Pitch Plane, Near Peak Heating. Angle of Attack: 39.59 degrees, Altitude: 227,424 ft (69.319 km), Mach: 22.91, Velocity: 22,505 ft/sec (6.8595 km/sec) at 13:54:24. Reynolds Number based on length: 1.18 million.

Owing to cooling of the shock layer gases in the boundary layer formed over the Space Shuttle and the TPS material response, the surface of the vehicle operates at temperatures (denoted by T_w) considerably lower than those in the shock layer. These data are displayed in Figure 2 (b). These temperatures depend upon the response of the TPS and typically range from 3,000 - 2,900 °F on the nose and in the area of the shock-shock interaction on the wing leading edge. The shock-shock interaction arises from the merging of the body shock with the shock layer formed on the wing leading edge. This merging causes enhanced pressure and aeroconvective heating in this region.

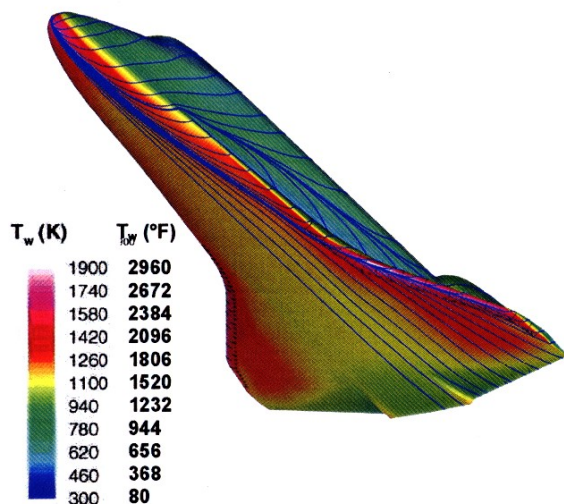


Figure 2 (b): CFD Solution for Surface Temperatures (T_w) with Streamtraces. Conditions as in Figure 2 (a).

From Figure 2 (c) displaying surface pressure, it is noted that the stagnation pressure near the vehicle's nose is 75 pounds per square foot (psf), dropping down to about 34 - 24 psf at the mid fuselage and aft fuselage locations, respectively. The shock-shock area, where the nose shock intersects the wing, runs at higher pressures (64 psf) than on the mid-belly region. Pressures on the top surfaces of the wings and fuselage sidewalls are near or below the free stream static pressure of 0.12 psf.

For comparison, Table 1 compares the gas and surface conditions for the Space Shuttle's entry environment at altitude to those on the surface of the Earth. Temperatures in the free stream are quite cold while those in the gas and on the vehicle's surface are extremely hot. Pressures are quite low, especially in the free stream at altitude as compared to near sea level (Palo Alto, California).

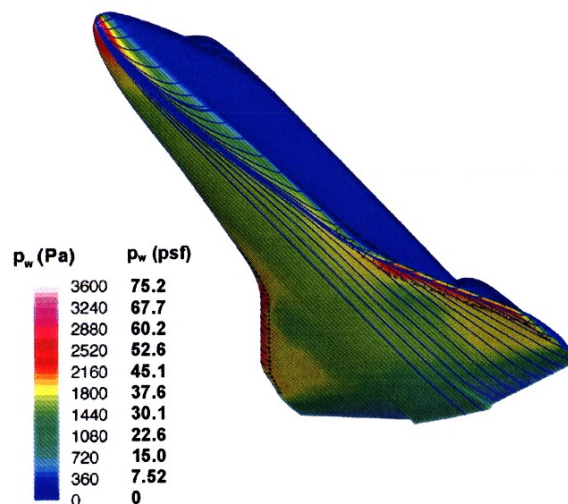


Figure 2 (c): Surface Pressure with Streamtraces. Conditions as in Figure 2 (a).

Location	Gas Pressure (psf)	Gas Temperature (°F)	TPS Temperature (°F)	Gas Speed (fps)	Number density (parts/cc)
Freestream	0.12	-61	-	22,400 (Mach 23)	2×10^{15}
Nose (stagnation)	75	22,000	2600	0	1×10^{19}
Mid-fuselage	34	12,500	1600	16,900 (Mach 3)	1×10^{18}
Aft fuselage	24	12,000	1350	16,600 (Mach 3)	1×10^{18}
Palo Alto, CA	2116	59	-	-	2.5×10^{19}

Assuming no ionization Assuming adiabatic back wall

*Local Mach number in flow

Table 1: Comparison of Vehicle Environmental Conditions at Peak Heating. Mach Number (Mach 23) to Ground Conditions.

Figure 3 is based on the CFD results from Figure 2. Here one sees zoom-in views of wall temperature and surface pressure distributions in the left wing leading edge area. Also shown are RCC panel locations. As can be seen, there is an attachment line along the wing leading edge where the flow divides, part going over the wing and part going below the wing. In both instances the flow is expanding into lower pressure locations. Along and near the attachment line, the principal direction of the flow at the surface is along the wing, in the outboard direction.

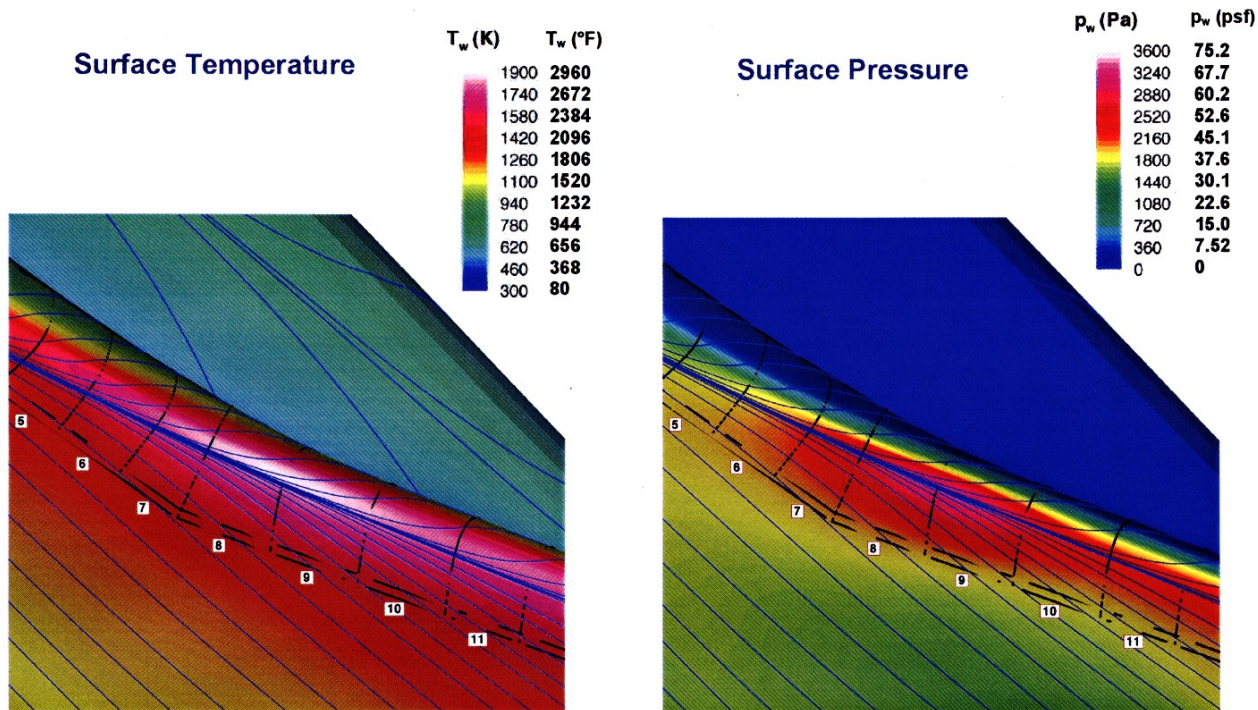


Figure 3: Zoom-in on CFD Solutions from Figure 2 in the Regions of RCC Panels 5-11.

Thermal Protection System TPS

From the previous section, one can understand the formidable problem facing designers of the Space Shuttle. A vehicle made of aluminum with its melting point of about 1000 °F would rapidly melt when exposed to the superheated air in the shock layer. Previous attempts to build a metal-skinned entry vehicle called Dynasoar using a hot structure approach had failed. The approach taken by the Shuttle Program in the late 1970's brilliantly solved this problem by dividing the problem into two parts that could be addressed independently:

- (1) Build a cool aluminum structure based on existing aircraft technology.
- (2) Solve the thermal problem with an external insulation tile system for acreage and a Carbon - Carbon hot structure approach for the nose cap and wing leading edges.

Figure 4 overviews the Shuttle TPS system with selected images from a comprehensive presentation (Reference 11) of the Shuttle Thermal Protection System TPS by NASA JSC TPS personnel, J. Kowal and D. Curry, delivered to the CAIB on February 10, 2003. As seen, the Shuttle's aluminum skin and structure are protected by a TPS configuration of RCC, a thermostructural material capable of reuse temperatures to 3,000 + °F on the wing leading

edges and nose cap; lightweight ceramic tiles with multi-use capabilities to 2,300 °F; and two types of blankets, Advanced Flexible Reusable Surface Insulation (AFRSI) capable of reuse temperatures to 1200 °F and Flexible Reusable Surface Insulation (FRSI) capable of reuse temperatures to 800 °F.

RCC consists of a carbon substrate made of graphitized rayon fabric impregnated with phenolic resin and pyrolyzed to convert the phenolic into the carbon matrix. To protect the carbon substrate from hot oxygen, a silicon carbide (SiC) coating of 0.02 - 0.04 inches thick on all surfaces is provided. It is over coated with silica, formed from Tetraethylorthosilicate (TEOS) and a Type A sealant of sodium silicate glass.

The Reusable Surface Insulation (RSI) tiles are made primarily from very fine silica fibers sintered together in densities of 9 to 22 lbs/ft³. Because of their low density and fibrous nature, they are extremely good insulators. RSI tiles are coated with a thin (0.012 inch) borosilicate glass coating called Reaction Cured Glass (RCG) which reradiates the incoming heat back into space. The design requirements for these tiles are that the bond line temperatures not exceed 350 °F at any time and that they are reusable for 100 flights.

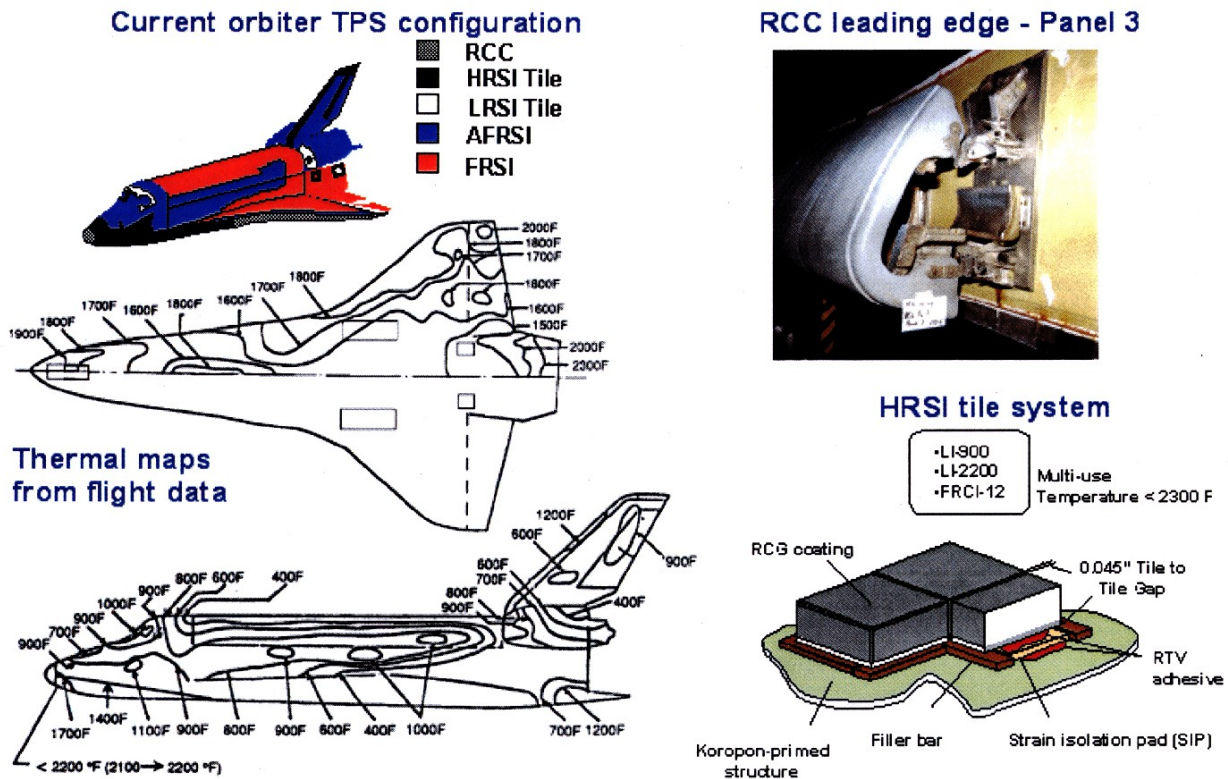


Figure 4: Overview of the Shuttle Thermal Protection System.

Thermal maps obtained from Orbiter Experiments (OEX) data early in the Shuttle Program, are shown in Figure 4. Also shown is a depiction of how the tiles are bonded to the Shuttle's aluminum skin. A photograph of a RCC wing panel (Panel 3) with the insulation, mounting attachments and the aluminum wing spar is also shown. Not used in the Panel 3 area are metal beams that span the open end of the RCC, from the top to bottom attachment points. These spanners are used in the Panel 8/9 area to provide additional strength. Note that there is a cavity behind the RCC and insulation between the RCC and the wing spar. This insulation protects the spar against radiation from the inside of the RCC. Not shown in this picture is the insulation that covers all internal metal surfaces ensuring that no structure is exposed to the radiation from the RCC. RCC has a very high thermal conductivity and therefore its inside surface is nearly as hot as the outer surface exposed to aeroconvective heating. During reentry, at an angle of attack of 40 degrees, the lower portion of the RCC panels receive most of the aeroconvective heating. The higher temperature lower panels are cooled by internal radiation through the cavity behind the RCC to the cooler top of the panels, which in turn radiates off to space. There are 22 RCC panels on each wing, and the gaps between them are

covered with flush-mounted seals, called T-Seals, owing to the cross-sectional shape of the seal.

To understand the events that occurred on STS 107, to be discussed below, it is important to note that the RCC-LESS cavity is vented. The venting is accomplished by a gap, ranging in width from 0.065 to 0.164 inches between the upper back edge of the RCC panels and the upper wing tiles. This gap runs the entire length of all RCC panels, giving a total vent area of 47 to 74 square inches depending on the actual gap widths. The smaller area corresponds to using the minimum allowable, installed gap width requirements and the larger area corresponds to using the maximum allowable, installed gap width requirements. Details of the gap design and width specifications are shown in Figure 5. The location of the gap was chosen because of the low heating rates and pressures that exist there as listed in Table 2. As can be seen, the pressure ratio peaks at RCC Panel 10 and falls off gradually in both the inboard and outboard directions. The fluid physics of the wing flow provides an extremely large driver pressure differential for a breach through the wing leading edge as illustrated by these pressure ratios.

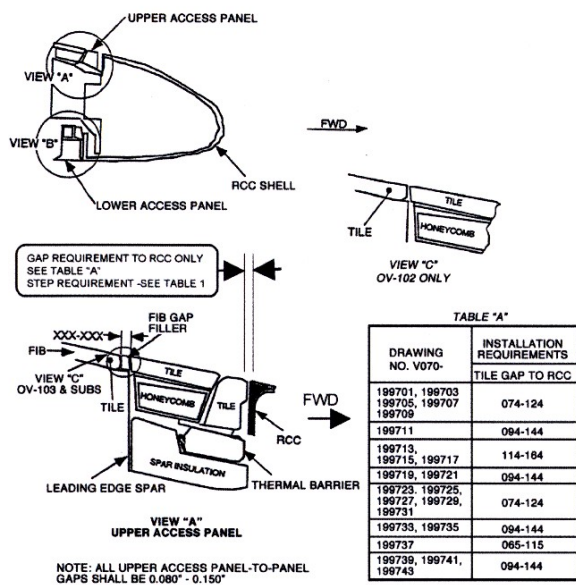


Figure 5: Details of Wing Leading Edge Subsystem Vent Design. Orbiter Vehicle (OV) 102 is named Columbia.

RCC Panel	Pvent/Panel 9 Peak	RCC Panel	Pvent/Panel 9 Peak
1	0.0048	12	0.0203
2	0.0052	13	0.0180
3	0.0053	14	0.0149
4	0.0053	15	0.0112
5	0.0063	16	0.0118
6	0.0082	17	0.0071
7	0.0083	18	0.0061
8	0.0115	19	0.0056
9	0.0210	20	0.0040
10	0.0255	21	0.0021
11	0.0228	22	0.0005

Table 2: Pressure Ratios for Leeside Surface Pressures at the WLESS Vents. Values at the Mid-point of the RCC Panel Trailing Edge. Ratios Normalized by the Peak Pressure on Panel 9 (3092.8 Pa or 64.6 psf). Results Based on NASA CFD Solutions for GMT 13:54:24, 227,424 ft, Mach 22.91 and Angle of Attack of 39.59 Degrees.

**ENTRY INTERFACE (EI) GMT 13:44:09 ->
13:47:30: Early Heating of Wing and Initiation of
Thermal Damage**

According to the hypothesis, the ET foam strike, which occurred at 82 seconds after lift off, compromised the RCC leading edge. Analysis of launch imagery (Reference 1) and state-of-the-art CFD (Reference 2) computing the transport of the foam within the complex flow field about Columbia, and its launch elements (External Tank, Solid Rocket Boosters and attachments) have shown that the foam strike occurred in the RCC 5-8

panel area. Both studies show that the strike was below the wing apex. The strike also occurred in the region of the shock-shock interaction area where reentry heating is high, as previously noted.

Testing at Southwest Research Institute and associated analysis has shown (Reference 3) that a strike of debris on the RCC from the ET bipod (briefcase-sized, weighing about 1.7 lbs) striking the WLSS at speeds of 770 ft/sec can cause severe damage. Damage observed included RCC panel cracking, cracking of T-Seals, displacements of both panels and seals and the formation of holes as large as 16 inches by 16 inches.

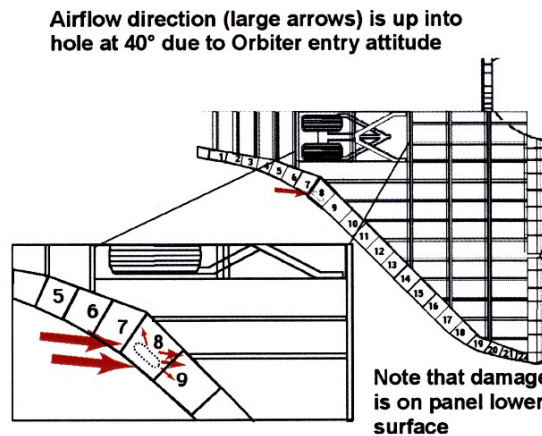


Figure 6: Hypothesized Entry Damage and Initial Entry Heating at Entry Interface.

Figure 6 depicts a breach (hole) in the lower RCC Panel 8. The view is down at the wing, looking through the top of the RCC panel. At entry interface, the flow is free molecular, and air molecules follow straight paths until they strike a solid surface. Assuming there was a hole in the lower part of Panel 8, the flow would be up into the hole, in the x-z plane of Columbia and at an angle of 40 degrees from the x-axis, corresponding to the angle of attack. The large red arrows show this flow direction in the plane of the paper (x-y) while the smaller red arrows show that there would be a "splash effect" when the air molecules strike the elements including insulation and metal mounting fittings inside the wing leading edge. Some of these elements are shown in the photograph in Figure 4.

As Columbia descended into the atmosphere, density increased and the free molecular flow transitioned to a continuum. As this happened, a shock wave formed over the vehicle giving rise to the flow field described above. In continuum flow, the flow vector is mainly along the wing surface instead of 40 degrees to the surface. For STS 107, superheated air from the shock layer entered the

breach and pressurized the cavity between the RCC and the insulated wing spar. Abnormal flow then exited out through the vents into the very low-pressure region at the top of the wing previously described.

Table 2, based on the CFD solutions discussed above for a normal condition corresponding to STS 107 at GMT 13:54:24, shows very large vent pressure ratios referenced to the lower side of Panel 9. Note that the ratios are large, ranging from 0.026 to .005 falling off from the Panel 9 - 11 area, both to the inboard and outboard direction. These ratios provide a very large driving potential to the internal flow.

One piece of evidence that corroborates that there was a breach in the wing at EI comes from the MADS/OEX thermocouple located behind the spar at the Panel 9 location. As discussed in References 4 and 12, there was “out-of-family” heating at this location during the STS 107 ascent. Figure 7 shows the time history of the measured thermocouple signal and the comparison of NASA’s thermal analysis (Reference 12) of the ascent event. As indicated on the figure, the “stepped” curve is the flight data while the blue-colored, smooth curve is the result of the NASA analysis. Note that the temperature readings are not large, owing to the facts that ascent heating is small, relative to that for entry, and that the thermocouple is behind the spar and the spar insulation. Detail of thermocouple locations will be discussed later.

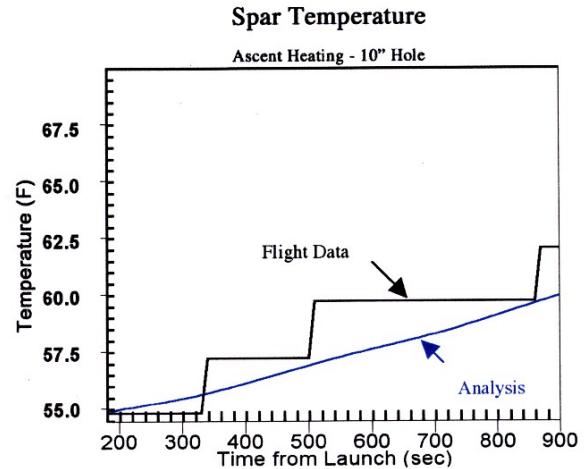


Figure 7: Data from OEX Thermocouple VO 9T9895 and Thermal Analysis by NASA (Reference 12).

NASA’s thermal analysis of the signal between 200 -> 900 seconds after launch suggests that ascent heating due to a hole of 6 – 10 inches in diameter in the wing leading edge can account for this anomalous heating. While this is not conclusive evidence that a breach existed after the foam strike at 82 seconds into the launch, it is quite consistent with the hypothesis.

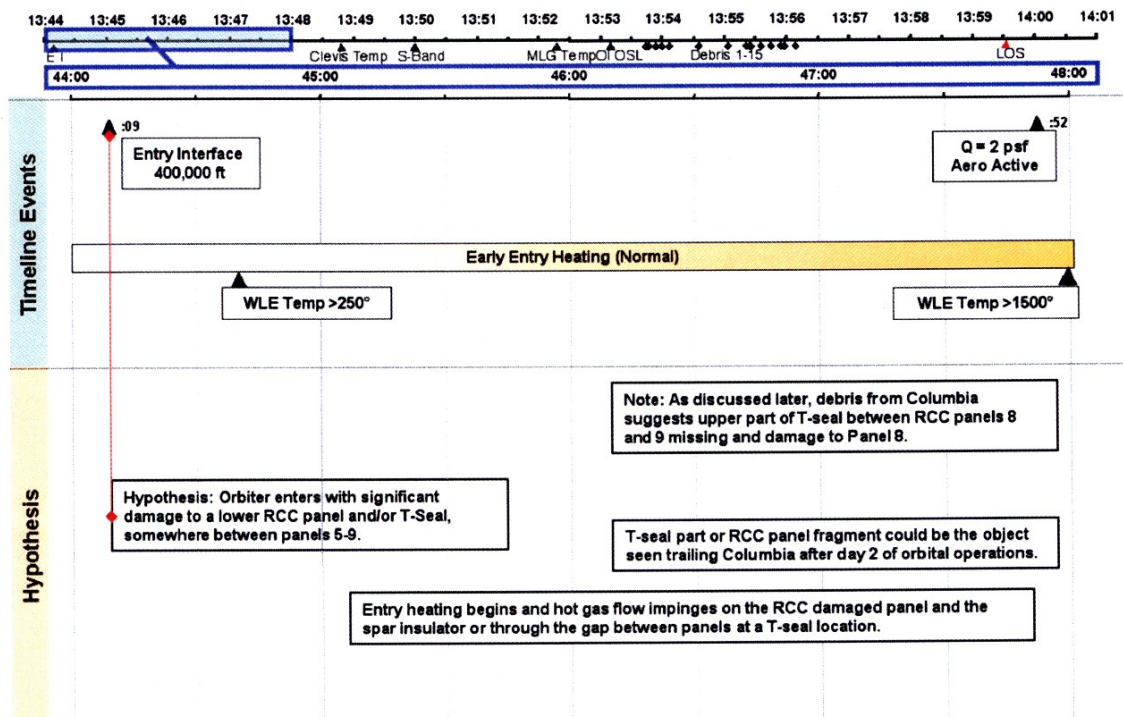


Figure 8: Timeline From EI 13:44:09 -> 13:47:30.

Figure 8 shows the comparison of timeline events from EI 13:44:09 to 13:47:30 to the hypothesis. This format, developed by NASA's Working Scenario Team (Reference 13), was adopted by the present authors. The format highlights portions of the entire sequence from EI through loss of signal (LOS) GMT 13:44:09 -> 13:59:32 shown at the top of the figure. The period being studied is highlighted with the blue rectangles, in this case 3 minutes and 21 seconds after EI.

Timeline events (tested and adopted as being "truth") appear on the upper half of the figure while those in the hypothesis (or scenario) are displayed in the lower portion of the figure. This figure shows the entry interface timing and wing leading edge heat-up for a normal wing during the expected STS 107 entry. In the lower part of the figure, the hypothesized damage to the lower RCC Panel 5-8 region as depicted in Figure 6 is noted, as is the beginning of the thermal attack on the wing leading edge subsystem. As discussed later, the debris recovered from Columbia strongly suggests the initial breach was in Panel 8, and the upper part of the T-seal between Panel 8 and 9 was missing or displaced.

ENTRY FROM 13:47:00 -> 13:50:00: MADS/OEX Data Show the Progression of Damage is From the RCC -> Aft

This section begins with a discussion of MADS/OEX sensor readings and then compares the interpretation of the data occurring between 13:47:09 until about three minutes later at 13:50:00 with the hypothesis.

Figures 9 and 10 depict the physical location of the MADS/OEX sensors in the Panel 9/10 area of Columbia's left wing. Figure 9 is a photograph of the backside of the wing spar, looking forward. The approximate locations of RCC Panels 9 and 10 are shown near the top of the photograph. Fortunately, this region of the wing on Columbia was instrumented for the Orbiter Experiments (OEX) activity early in the Shuttle Program, and the instruments were still operational and recording data during STS 107. Data from four sensors are extremely valuable in helping understand the temporal events leading up to the failure of the wing leading edge system: V12G9921, a strain gage mounted to the spar; V09T9895, a thermocouple mounted to the back of the spar at the Panel 9 location; V09T9910, a thermocouple mounted to the clevis which held RCC Panel 9 in place (under an "earmuff" which insulated the clevis); and V0T9666, a thermocouple mounted in a tile in the lower wing, near the tile surface, close behind the number 9 carrier panel tiles. V09T9910 is imbedded in the RCC mounting hardware, which secures the panel to the spar.

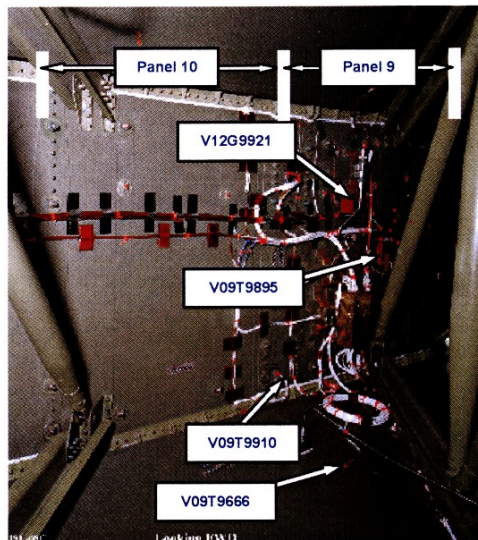


Figure 9: Photograph of Rearward Side of Columbia's Left Hand Wing Spar, Looking Forward. OEX Sensor Locations are Depicted.

To help visualize the geometric location of the sensors, Figure 10 shows portions of an engineering drawing from a document describing the OEX instrumentation. As can be seen, top and side views are shown along with a key identifying the type of sensor.

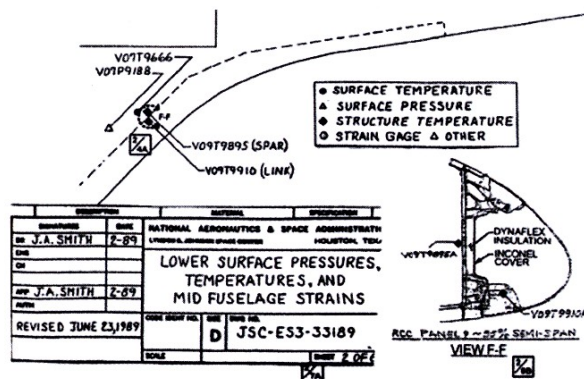


Figure 10: Portion of an Engineering Drawing Depicting the Location of OEX Sensors.

Figures 11 through 13 show data from the two sensors (one strain and one temperature) discussed in Figures 9 and 10. The information from these sensors is very significant in determining the progression of events as the thermal damage from the initial breach progressed to burn a hole through the wing spar. In addition to the data

obtained on STS 107, sensor traces taken on other flights, with similar entries are displayed with different color codes. Other investigators have made detailed analyses of these signals and data from many more sensors, but herein, only major events, appropriate to our “Follow the TPS” theme are discussed. In each plot, there is an indication of the first off-nominal or “out-of-family” event that will later be used in comparing flight data to the hypothesized events causing loss of vehicle and crew. The units in Figure 11, measured by the temperature compensated strain gage are micro inches/inch.

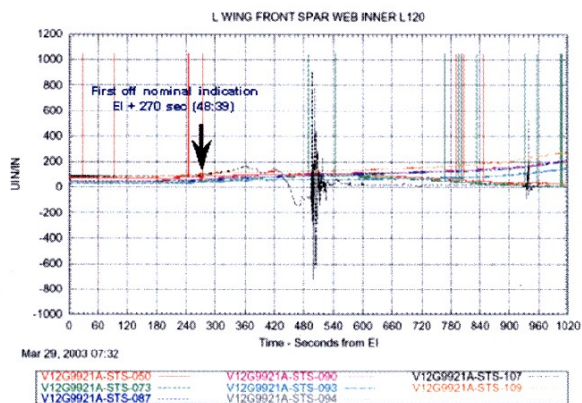


Figure 11: OEX/MADS STS-107 Flight Data.

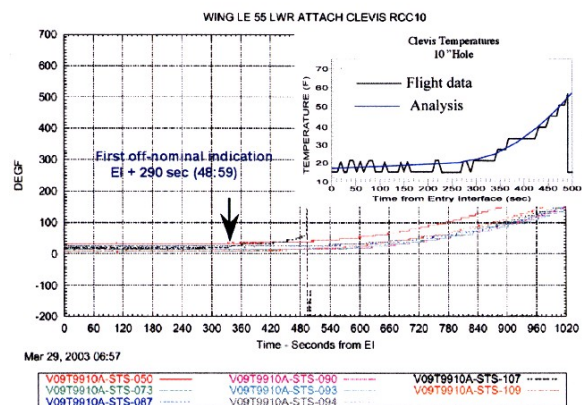


Figure 12: OEX/MADS STS-107 Flight Data and Thermal Analysis (Reference 12).

Figure 12, prepared in the same format as Figure 11 displays the time history of a thermocouple imbedded in the clevis fastener at the lower edge of the RCC located between Panels 9 and 10. The temperature changes recorded on the RCC clevis during STS 107 entry, appear to be quite small, but it is noted that this thermocouple is highly insulated and attached to a large thermal mass.

A thermal analysis by NASA (Reference 12) has shown that a hole of 6 -> 10 inches in diameter in the lower RCC Panel 8, could account for the early behavior of the thermocouple. The result of this analysis is shown in the inset in Figure 12. The “stepped” curve is the flight data while the blue, smooth curve is the result of the referenced analysis.

Figure 13 shows temperature histories from the left-hand Orbital Maneuvering Systems (OMS) Pod. Again, data from other, similar flights is shown. As can be seen, below nominal temperatures were recorded, starting at about 340 seconds after EI. The following figure explains that this is likely due to a modification to the normal flow field by damage in the wing leading edge. Note also from this figure that at about 540 seconds from EI, the temperature abruptly increases, to values well beyond that for a normal entry.

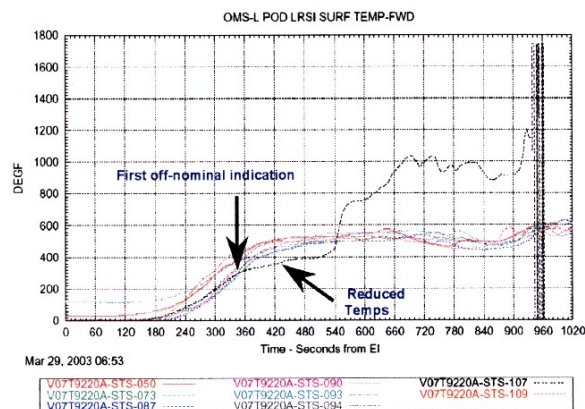


Figure 13: Off-nominal OMS Pod Temps.

Figure 14, prepared by NASA (Reference 14) shows the results of wind tunnel tests from Langley Research Center. Data were obtained in a Mach 6 air stream at the conditions specified on the figure. The three boxes on the right of the figure show the results of a thermally sensitive coating on a model of the Shuttle. As noted, for the results of RCC Panels 5 and 10 missing, there is a definite temperature decrease from the baseline on the left OMS pod location, noted by the absence (missing panel number 5) or dimming of the red dot on the forward location of the OMS pod. The conceptual sketch, also shown in Figure 14, suggests that the jet-like expansion directed from a damaged wing influences the leeside flow field, reducing OMS heating if there is a disturbance in the Panel 5-10 RCC area.

While this simulation does not duplicate flight conditions, the trends do help explain the below nominal

temperatures of the OMS pod seen in the OEX data. NASA Ames has also produced (Reference 7) CFD results supportive of the trends identified, in the wind tunnel testing, using the GASP CFD code previously described (Reference 9).

Figure 15 graphically depicts the timing of events recorded by the OEX sensors. The captions are self-explanatory. The MADS/OEX off-nominal data in the wing leading edge and spar are additional evidence that a breach existed in the RCC at the EL. The below nominal temperature on the OMS pod is consistent with the hypothesized damage in the wing leading edge in the RCC Panel 5 - 8 area.

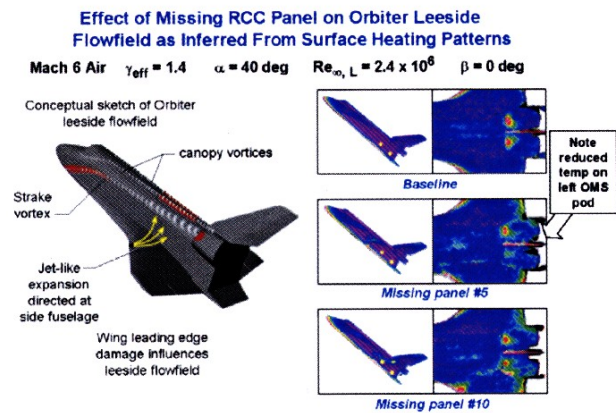


Figure 14: NASA Langley Wind Tunnel Test Data Help Explain Below Nominal Temperatures Recorded on the Left OMS Pod.

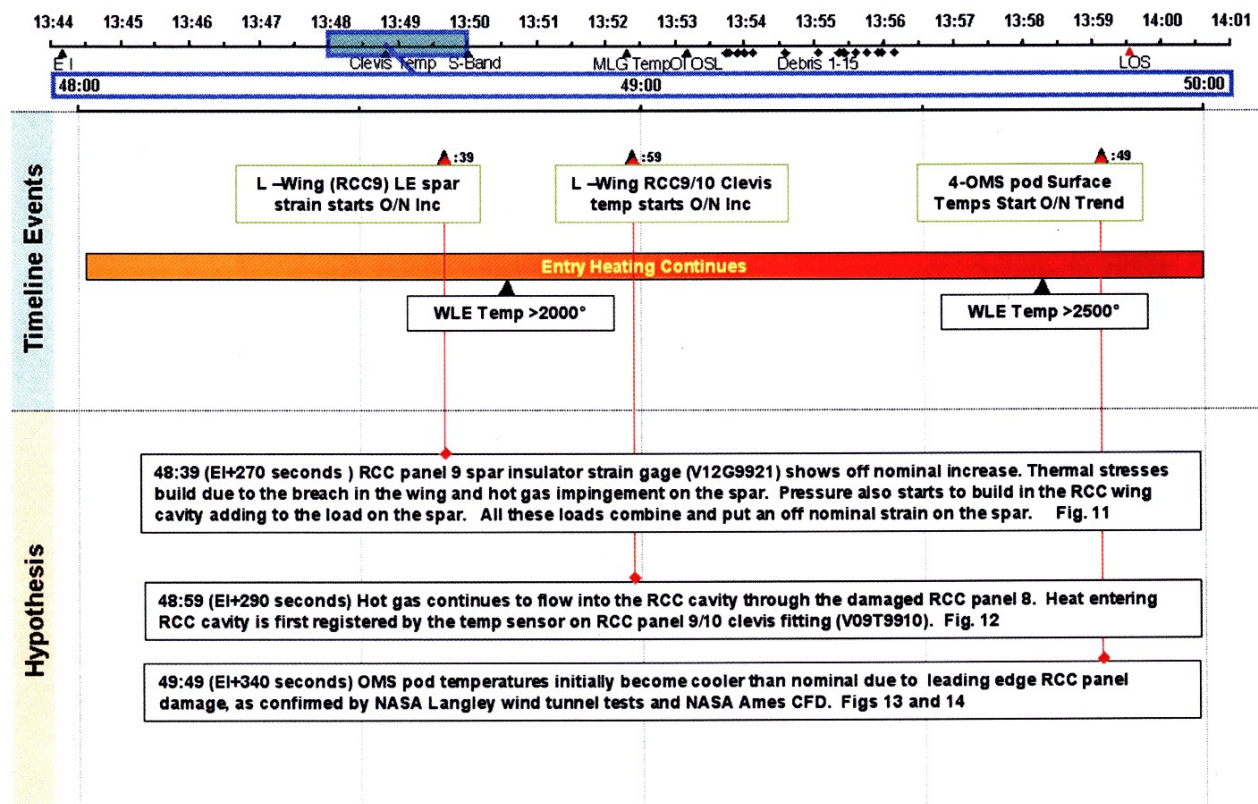


Figure 15: Timeline Versus Hypothesized Events 13:48:00 -> 13:50:00.

ENTRY FROM 13:50:00 -> 13:52:00: Entry Events Through Spar Burn - Through

Figure 16 depicts a possible explanation for some of the early (near 13:50:00) communication dropouts observed during Columbia's entry. As known from many years of experience with entry of vehicles, small amounts of charged species (electrons and ions) between an antenna and the receiver can cause communication signal attenuation and even its total loss. As shown in the figure, a possible explanation for some of the early signal attenuation could have been electrons and ions, along with molten materials from the wing hardware, being entrained in the flow and transported to locations between the antennae behind Columbia's cockpit and the receiving TDRS communications satellite.

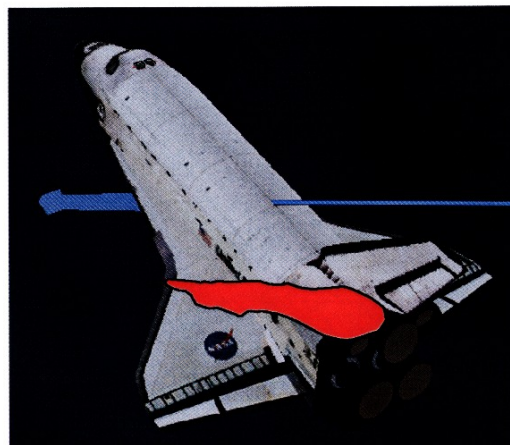


Figure 16: Entry Plume is Possibly Affected by Damaged Structure Accounting for Communications Dropout.

At the request of the authors, D. Potter of Sandia National Lab performed a scoping study (Reference 15) which shows that melting aluminum would provide charged species concentrations in sufficiently large quantities for signal attenuation in the 13:50:00 -> 13:50:30 period. However, to date (July 2003) analysis by NASA has failed to provide an understanding of how the flow behind Columbia could have provided a pathway to place the charged species and/or molten metal between the antennae and the receiving satellite. Darling (Reference 4) has pointed out that the communications drop out occurred at times quite close to several major debris shedding events and to the breach of the LW spar. However, a definitive link between the two is still conjectural.

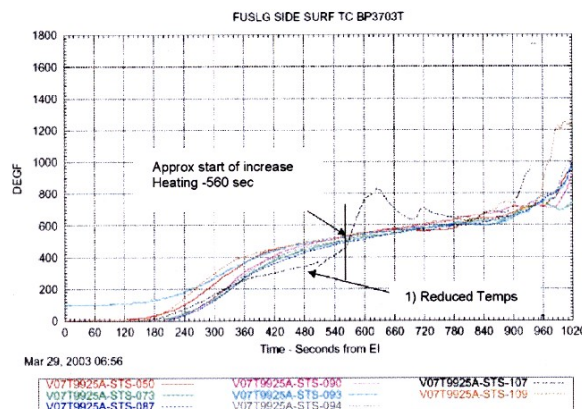


Figure 17: Representative Fuselage Sidewall Thermocouple Data.

Figure 17 displays the left fuselage sidewall thermal profile for thermocouple VO7T9925A in the standard MADS/OEX format wherein the data for STS 107 are compared to those from other, similar entries of Columbia. As can be seen, there is an out-of-family lower temperature trend at EI + 360 seconds, correlating to GMT 13:50:09. This early below nominal, and later, above nominal temperature observation on the fuselage sidewall, for a number of thermocouples has been explained by the NASA team led by J. Caram (Reference 16) to arise from flow disturbances propagated from the wing leading edge. The study depends upon a combination of hypersonic wind tunnel data and CFD analysis. The reader interested in detail is referenced to this report and the Aerothermodynamics section of the CAIB report (Reference 17).

Figure 18 displays the temperature recording from the thermocouple VO7T9666A located in a lower wing tile, near the wing leading edge, behind Panel 9. This sensor location was shown above in Figures 9 and 10. As can be seen, there is an off-nominal heating trend in this thermocouple starting at EI + 370 seconds (GMT 13:50:19).

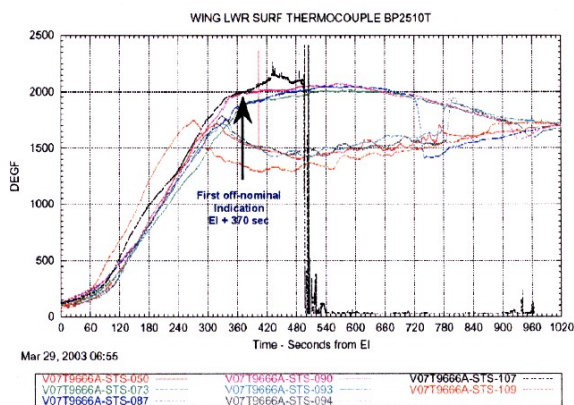


Figure 18: OEX/MADS STS-107 Flight Data.

As shown in Figure 19, thermocouple V07T9666A is in the flow area affected by Panel 8 (Reference 18). Specifically, as shown in the figure, the streamline, which passes over the junction of the lower Panel 8/9, also intersects the approximate location of this thermocouple. As will be discussed below, the forensic analysis shows compelling evidence that there was an outflow from the aforementioned 8/9 RCC lower panel junction that probably caused the above nominal readings of V07T9666A that started at EI + 370 seconds and continued till the spar breach occurred. This CFD solution by Gnoffo, Alter and Thompson (Reference 18), was the starting point of studies of flow into the breach, as will be discussed below.

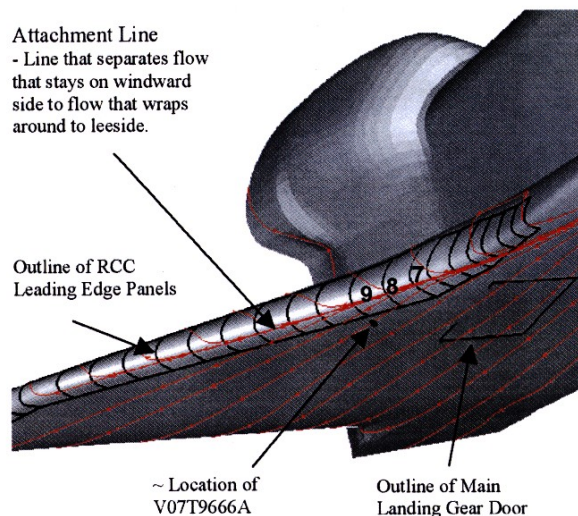


Figure 19: Orbiter Surface Streamlines. 13:50:53 (EI + 404), Mach: 24.9, Altitude: 243 k ft and Location of Thermocouple in Tile. CFD Solution from NASA (Reference 18).

Figure 20 displays the temperature recordings from thermocouple V0T9895A, located on the inside of the spar, behind Panel 9, as discussed in Figures 9 and 10 above. These data are quite valuable in understanding the progression of damage to the wing leading edge. As seen, the first off-nominal indication begins at 420 seconds after EI, GMT 13:51:09 with a very slight increase in temperature. Later discussion of this figure will focus on the burn through of the spar.

Figure 21 graphically depicts the timing of communication drop out and additional events recorded by the OEX sensors. The captions are self-explanatory. The MADS/OEX off-nominal data in the wing leading edge and spar are additional evidence that a breach existed in the RCC at the EI. The below nominal temperatures recorded on the fuselage sidewall is consistent with the hypothesized damage in the wing leading edge in the RCC Panel 5-8 area. The spatial correlation by the streamline analysis in Figure 19, showing how the outflow from the lower juncture of RCC Panel 8 and 9 can affect the lower tile thermocouple behind Panel 9 and the above nominal behavior of thermocouple V07T966, is additional and compelling evidence for the existence of a breach in the Panel 8/9 area. It is clear from this figure that the temporal evolution of the heat flow shows that the hot gas penetration began in the cavity in the wing leading edge prior to heating in the wing box behind the spar.

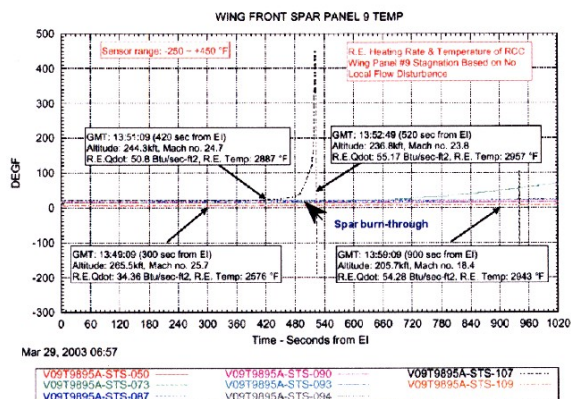


Figure 20: OEX/MADS STS-107 Flight Data.

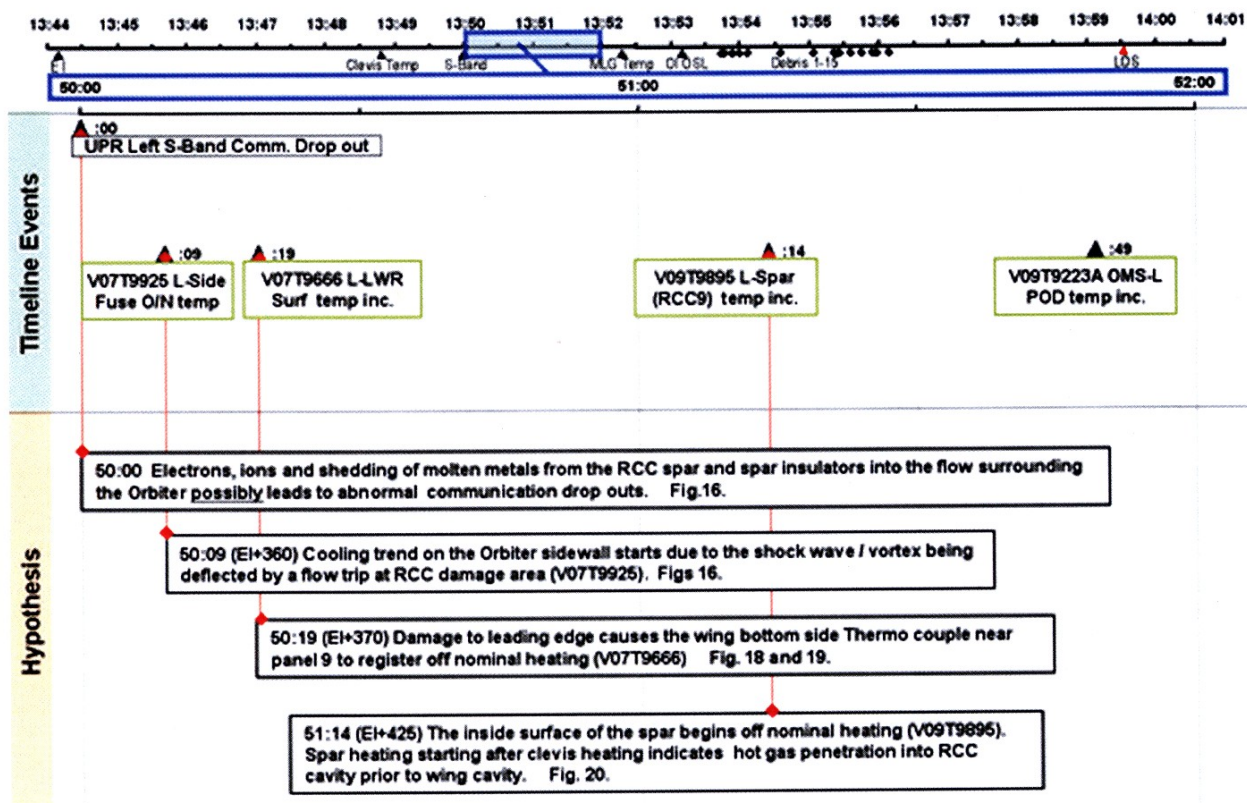


Figure 21: Timeline Versus Hypothesized Events – 13:50:00 to 13:52:00.

**ENTRY FROM GMT 13:52:00 -> 14:00:00
(Includes Spar Burn-Through to Loss of Signal)**

Figure 20 shows a rapid temperature increase at EI + 487 seconds as recorded by the thermocouple V0T9895A on

the back of the spar behind Panel 9. This rapid increase at EI + 487 seconds strongly suggests an appearance of a plume of superheated air and that spar penetration had occurred. According to study (Reference 13 and 19) by NASA, this timing for spar burn-through is consistent

with a thermal analysis for a 6 -> 10 inch diameter hole in the RCC Panel 8, failure of the leading edge wire harnesses and bit flips observed in the wheel well.

Figure 22 and 23 are artist's concepts of the burn-through and hot gases filling the wing box.

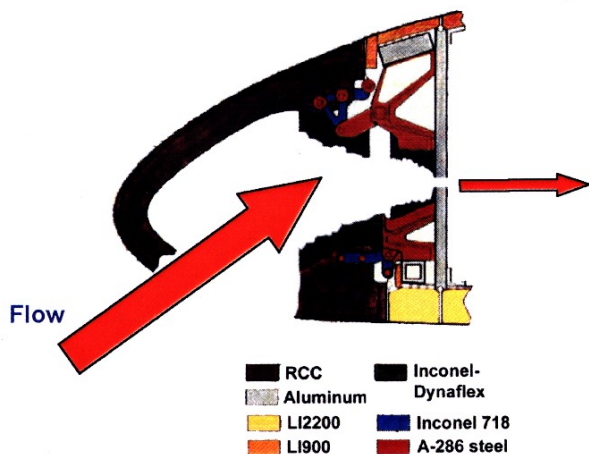


Figure 22: Spar Breach Occurs at EI + 487 Seconds.

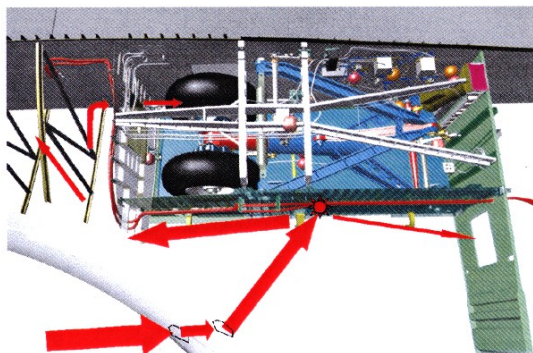


Figure 23: Hot Gas Begins to Fill Wing Box.

Figure 24 displays the time history of thermocouple V07T9220A located on the OMS Pod. The observation made by NASA (Reference 16) is that from 13:53:29 -> 13:55:29 (EI + 560 -> 680 seconds), there are continual off-nominal increases in OMS Pod temperatures that correlates with the timing of debris sightings 1-13 during the flight. This correlation clearly suggests increasing damage is occurring to the left wing, specifically to the TPS and its substructure.

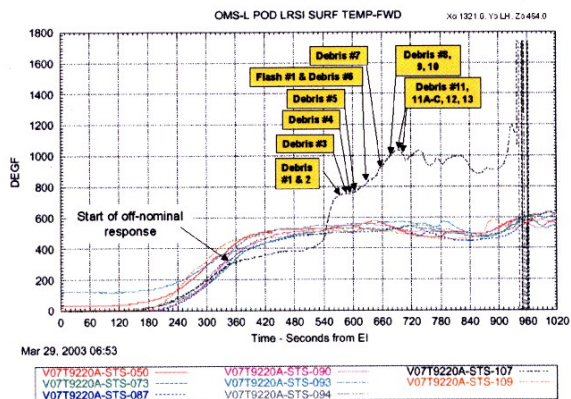


Figure 24: Left OMS Surface Temp Response Indicating the Progression of Damage.

Figure 25 is a photograph of Columbia, taken at GMT 13:57:14 from the Starfire Facility at Kirtland AFB in Albuquerque, NM. At this time, Columbia was about 50 miles NW of Starfire at an altitude of about 40 miles, it had an 80 degree left angle (with the left wing down) and a 40 degree angle of attack. Therefore, the view of the vehicle is from the forward, bottom, left side, so that any hot plumes spilling over the top of the left wing leading edge or out of the top of the wing near the leading edge are visible.

The image records the appearance of the shock layer around the vehicle. As is indicated by the model grid overlay, the left side of the fuselage would be visible if it were not for the shock layer brightness and the slight wrapping around of the flow over the lower part of the forward fuselage. The apparent enlarged portion of the nosetip area is also due to the shock layer expanding around the forward fuselage from the stagnation point at the lower part of the nose cap. The shock layer is also visible through the short (a few meters long) wake that persists behind the vehicle.

The left wing has two apparent "bulges" on the leading edge and two corresponding wakes behind the wing. The authors believe that these are due to the following: hot flow and burning material ejected upward over the wing leading edge from the Panel 8 area; and a large plume of hot gases and burning material and debris ejected upward from the breach in the top surface of the wing aft and outboard of the Panel 9/10 area.

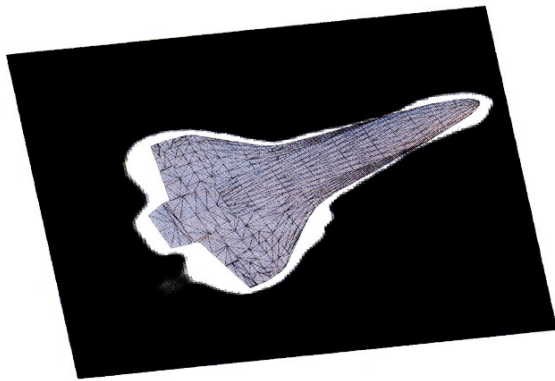


Figure 25: Starfire Photo from Kirtland AFB. GMT 13:57:14. Model Scaling and Orientation Based on Telemetry from NASA. The Columbia Model was Provided by NASA.

The captions within Figure 26 displaying the comparison to the hypothesis and the timeline between GMT 13:52:00 and 14:00:00 are self-explanatory. During this time, the breach through the spar and internal heating to the wing box and wheel well have rendered the loss of the vehicle inevitable. The temporal progression of damage to the TPS has been outlined herein with the exception of the shedding of tiles and RCC panels/parts. Geographic locations of the recovered TPS debris and ballistic analysis suggest that much of this occurred over Texas. Others have written in detail on the analysis of debris sightings, sensor readings, etc. and it is outside the scope of the “Follow the TPS” charter to dwell further on these topics.

In the following section one can see a detailed analysis of Columbia’s TPS debris and what it infers.

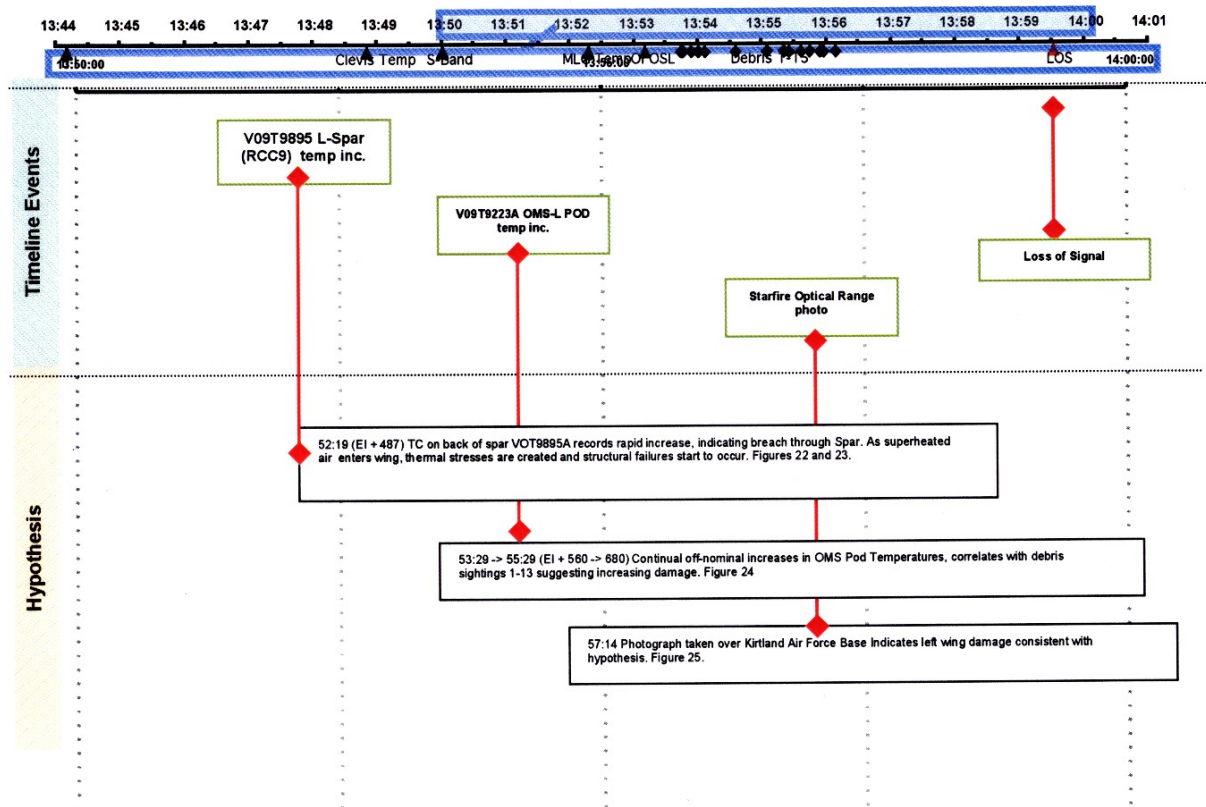


Figure 26: Timeline from 13:50:00 Through Loss of Signal 13:59:32 Versus Hypothesized Events.

TPS Debris and Forensic Analysis

In keeping with the "Follow the TPS" theme of this appendix, the focus herein is on the TPS debris and what story it tells about the demise of Columbia's RCC wing leading edge subsystem and tiles.

Figure 27, (Reference 20) provides a graphical description of debris recovered (as of April 30, 2003) from the left wing of Columbia in the RCC Panel 1 -> 11 region.

The following description provided to the authors by M. Ehret explains the symbols: Red means "Bad or Hot," Yellow is "So-So" and Green is "Good."

Note that one upper carrier panel tile from Panel 8, depicted by a "red" rectangle was slumped, showing evidence of prolonged heating. The paucity of upper carrier panel tiles in the 8/9/10 area may have been caused by hot gases exiting from the LW cavity volume through the vents between the upper rear portion of the RCC

flanges and tiles. This hot flow, containing melted materials from the interior RCC, would have had a very aggressive erosion effect on the upper carrier panel tiles and their attachments.

For "Slag" the diamond symbol was used: Red (H) means heavy slag, Orange (M) means medium slag, Yellow (L) means light slag, Green (no letter) means none or very light slag. "Holes without fractures" refers to the unbroken holes in the RCC, interpreted as evidence that the Inconel fasteners melted out. Here, red circles indicate that prolonged heating occurred. Red triangles depict significant RCC erosion. Green triangles indicate no RCC erosion. "Fractures" indicate the possible evidence of hot-shortcracking of the A286 carrier panel attach bolts (as evidenced by intergranular fracture) as an indicator of prolonged high temperature exposure (Reference 20/Appendix, by L. Korb). The red square represents the only such finding among these debris.

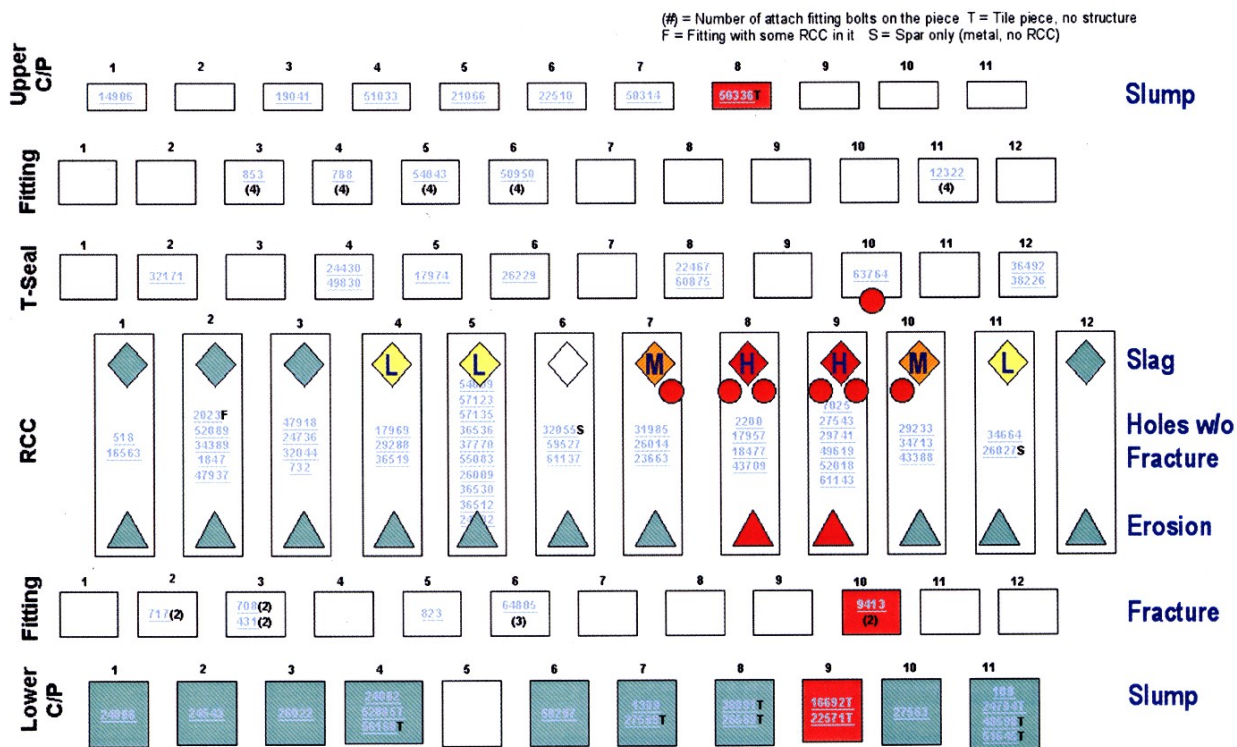


Figure 27: Left Hand Wing Debris Points to Breach in RCC Panel 8/9 Area (Reference 20).

Only lower carrier Panel 9 tiles showed the heavy slumping (red box). All other lower carrier panel tiles found as of 4/30/03 had no evidence of prolonged heating (Green).

In general, Figure 27 shows accumulated evidence that **only** the RCC Panel 8/9 region suffered PROLONGED heating. There is only one area on either wing where the attachment holes in the rear of the RCC panel flanges and ribs are intact (no fractures through the holes) and the attachment metal parts have been melted out. This is in the Panel 8/9 area of the left wing, indicating extreme heating conditions that completely melted out the Inconel fittings and in some cases even severely eroded the RCC mounting holes. All of the other recovered mounting holes in the RCC have either been fractured (the metal parts torn out) or the metal parts are still attached.

The photograph in Figure 28 is an outboard view of recovered parts of RCC ribs from Panels 8 and 9. For perspective, four recovered parts of the outboard rib of Panel 8 are shown sitting on white foam blocks: one upper part of rib 8, and three parts from the lower part of the rib 8 heel/lug bolt area. Two recovered parts from the inboard, upper rib of Panel 9 are shown laying on their full-scale drawing. A third part, placed on the drawing, not identifiable, is likely also from the inboard rib 9 in the location shown. Lack of positive identification of this part is indicated by the ? mark written on the yellow tag. These parts show heavy ablation, and the RCC LW LESS Panel 8/9 area is the only location found with this feature. Ablation features are labeled using yellow tags with the letter "A." The ablation patterns facing the camera on this side of the rib parts strongly suggests that superheated air had been flowing inside the wing, in a generally outboard direction. This indicates significant and prolonged flow from the Panel 8 area into the Panel 9 and outboard regions of the wing inside the RCC-LESS channel. Edges of the ribs are sharpened to a near "knife-edge" (0.05 inches compared to undamaged thickness of 0.365 inches), with a flat side away from the flow direction. Because of the durability of RCC and the extent of the ablation, this flow probably was sustained inside the RCC-LESS cavity area for hundreds of seconds. This type of damage is the result of oxidation (ablation) of the RCC carbon substrate. The following figure shows the same parts from an inboard view.



Figure 28: RCC Panel 8/9 Ribs (Outboard View).

Figure 29 is a photograph showing an inboard view of recovered parts of RCC ribs from Panel 8 and 9. Here, the two recovered and identified parts of the inboard rib of Panel 9 are sitting on white foam blocks. The recovered parts from the outboard rib of Panel 8 described in Figure 28 are now shown lying on their full-scale drawing. Note that the yellow tags here are labeled "NA," meaning not ablated and verifying the statements made in the discussion of Figure 28.

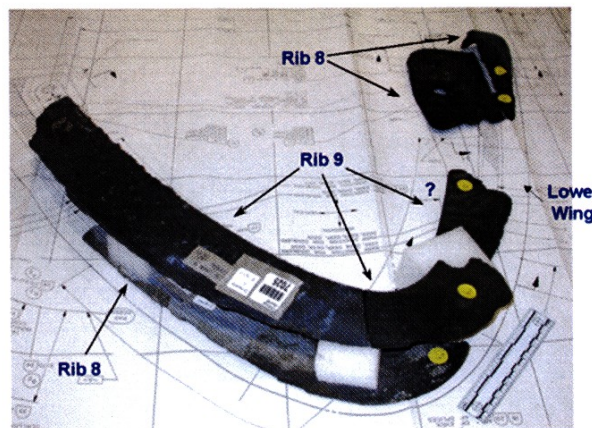


Figure 29: RCC Panels 8/9 Ribs (Inboard View).

Figure 30 is a photograph of the reconstructed left lower wing area of Panel 8/9. All parts shown are positively identified except for the "8/9" lower panels and the partial T-seal. Other left wing debris panels (16 and 17) were placed in the reconstruction to help visualize the original configuration. At the time the photograph was taken, the T-seal fragment was thought to be the T-seal which fits

between Panels 8 and 9, but later (4/26/03) thought to be from the 10/11 T-seal location. Definite identification of this T-Seal has been elusive and apparently is not possible (Reference 20/Appendix). Shown in the upper part of the photograph, in its approximate location, is the upper part of Panel 8. Note the slight flow patterning (possibly silica glass formed from the SiC coating) melt toward the upper part of the wing. This indicates that this was a late fracture, and that the exposed edge was in a super-heated air flow for a shorter time compared to the rib fragments shown in Figures 28 and 29. Note that the two LI 2200 carrier panel tiles below Panel 8 are in very good condition, while the three from the Panel 9 location show very heavy flow patterning, going in the inboard -> outboard direction. Close inspection of the heel area of outboard, lower Panel 8 shows a thumb-sized relief slot that was manufactured there to accept an inner panel thermal barrier. Hot flow exited out through this slot, causing the flow patterning on the three Panel 9 carrier panel tiles. The Panel 8 carrier panel tiles were not damaged, because they were protected by the lower Panel 8 and flow followed the direction of the external wing

flow streamlines (Figures 2, 3 and 19). These findings are consistent with the erosion patterns observed in the internal flow patterns in the actual 8/9 ribs discussed above.

As discussed earlier in describing Figure 19, streamline patterns determined by CFD show that flow out of this lower RCC Panel 8/9 juncture area directly affect the thermocouple V07T9666A, located in the lower tile field, close behind RCC Panel 9. This flow relationship, strongly suggests the above nominal temperatures recorded by this thermocouple were caused by the flow out of the lower Panel 8/9 juncture, which also eroded the lower Panel 9 carrier panel tiles. The flow out of this slot, into a relatively high-pressure area (but below the pressure at the inlet breach) was probably the only outlet available to the large volume of ingested gases once the flow-through of the RCC vent slots was choked. The traces in Figure 18 suggest that this started at EI + 370 seconds and persisted until spar burn-through at approximately EI + 487 seconds.

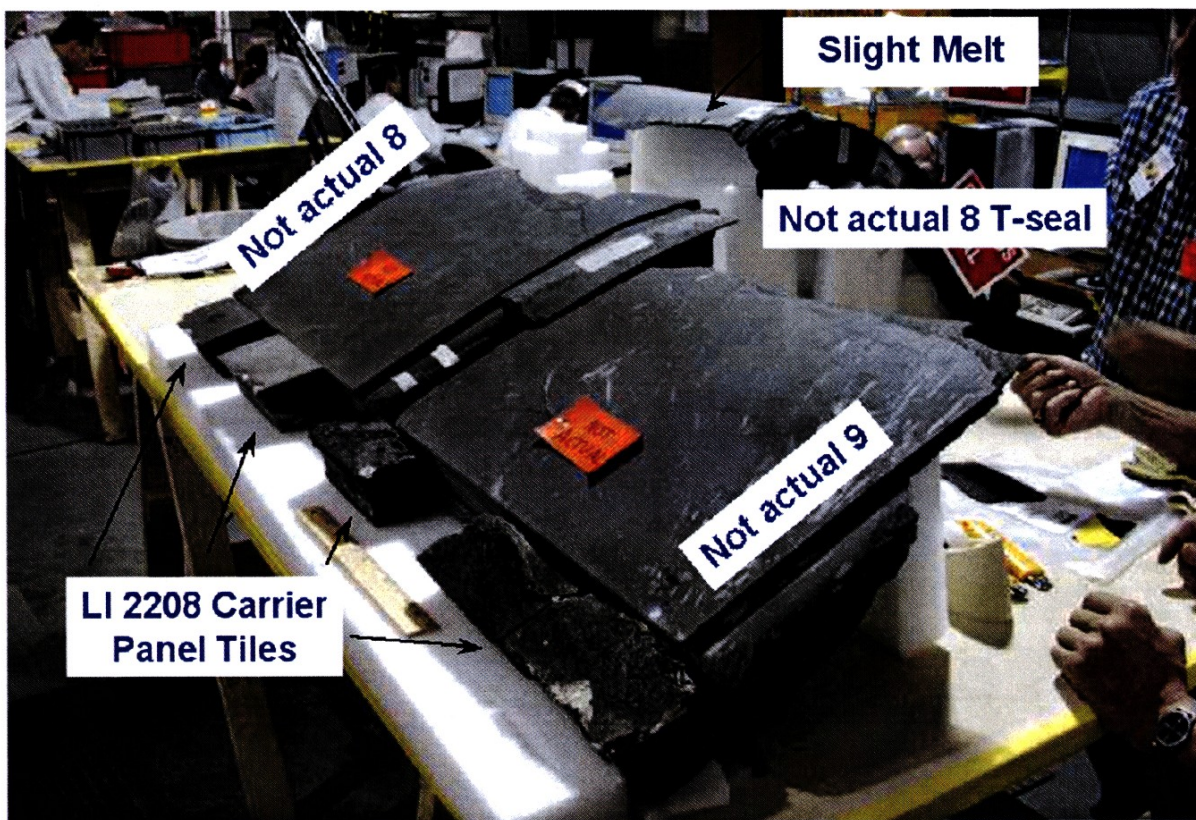


Figure 30: Reconstructed RCC Panel 8/9 Area.

The photograph in Figure 31 is a close-up of the slot in the heel of the outside, lower Panel 8 rib, manufactured there to accept an internal thermal barrier for the wing leading edge system. When hot flow existed inside the wing at the Panel 8 area, it created a “sneak” flow out of the wing causing the flow patterning on the Panel 9 lower carrier panel tiles previously described. There is also flow patterning on the side of the tiles facing the inner, lower part of RCC Panel 9 suggesting a channel flow there. This is not shown in this photograph.

Figure 32 is a close-up photograph of what was the RCC side of the vent gap on the upper Panel 8. See Figure 5 for an assembly drawing of the vent. As can be seen, there is a heavy accumulation of slag (up to 0.4 inches thick). This indicates that the gap at the top and outboard edge of Panel 8 and possibly Panel 9, were opened up from their normal configuration (0.114 to 0.164 inches) to at least 0.25 to 0.4 inches, and that melt from the interior fittings and insulation deposited there as the superheated air attacked the interior components of the WLESS and exited out of this vent location. The opening of the vent spacing could have happened at the time of the foam strike, or as the wing began to deform at the time of break-up; but most probably, it occurred during the long, high heating portion of the flight.

Figure 33 shows the probable initial breach location on the lower Panel 8 area. The size of the hole is difficult to determine, but could be bounded by the three dotted locations outlined by white tape. Analysis by NASA discussed above suggests the damage is consistent with a hole of 6 → 10 inches in diameter. All of these are consistent with the flow patterning seen on the debris and the Computational Fluid Dynamics flow calculations to be discussed below. The authors note that areas this large would be consistent with the “piece” shown by DoD radar observations that “left” Columbia on day two of its orbital maneuvers. A part of a broken T-seal (possibly from Panel 8, located between Panels 8 and 9) could also account for the “piece” observed leaving the shuttle on day two of orbital operations. Note that on this photograph, the two recovered Panel 8 carrier panel tiles are not shown.

The authors believe that in addition to a breach in Panel 8, the upper part of the T-seal between Panels 8 and 9 must have been missing or severely misaligned for a major part of the entry. This is required to account for the severe erosion of the upper RCC Panel 8 outboard and Panel 9 inboard ribs shown in Figures 28 and 29 and discussed above. Flow patterns of the recovered upper Panel 8, suggest this happened as discussed in Reference 20.

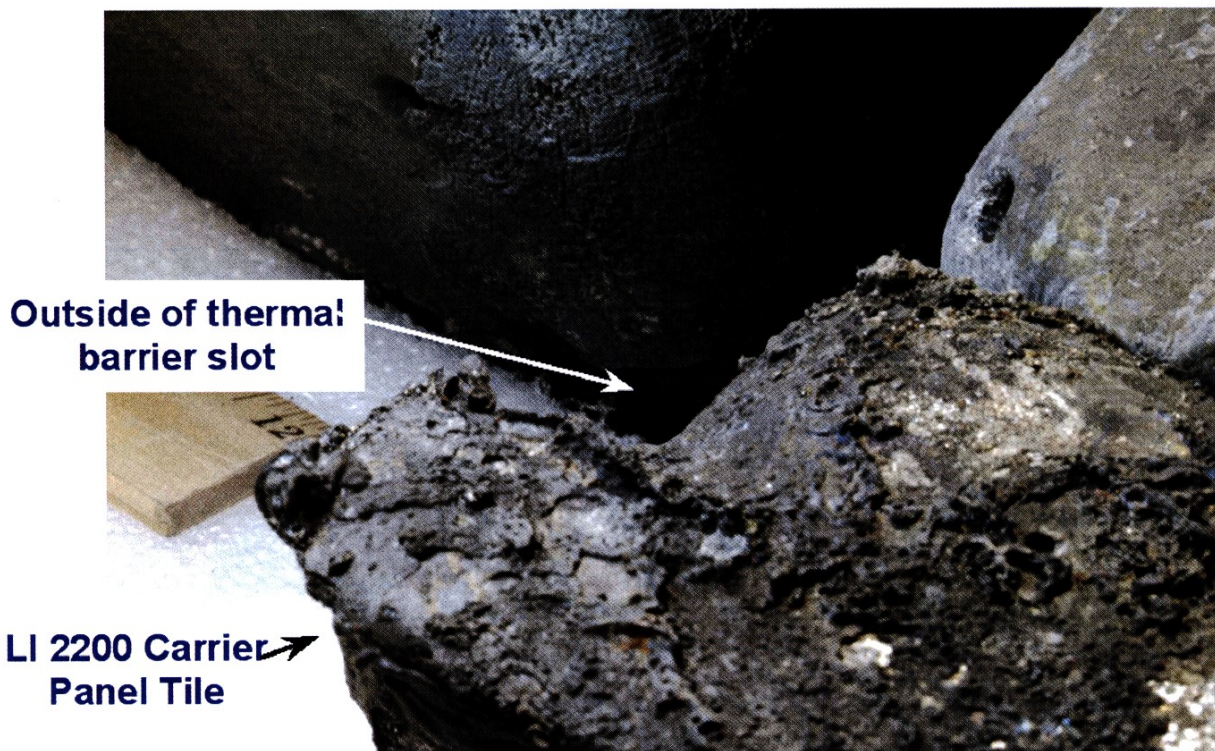
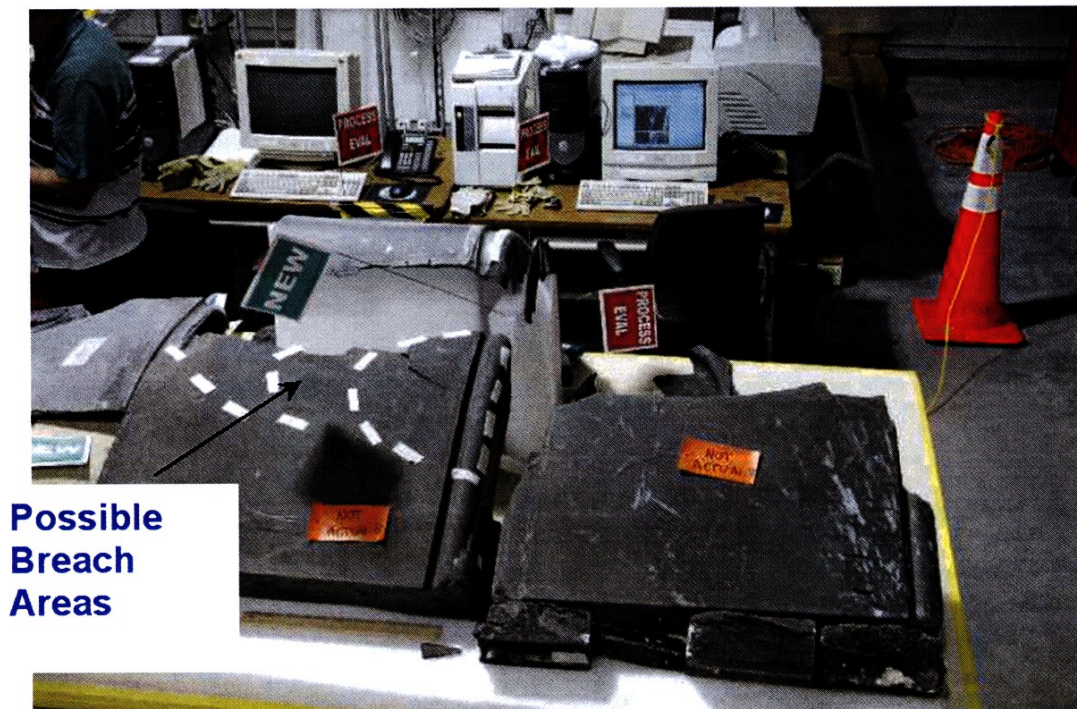


Figure 31: Close-up of Flow Location Affecting Panel 9 Carrier Panel Tiles



Figure 32: Slag Deposits on Upper Edge of Panel 8 on the RCC Side of the Vent.



**Possible
Breach
Areas**

Figure 33: Probable Initial Breach in Panel 8.

**Chemical and X-Ray Analysis of Debris
from RCC Panels**

Figure 34, adopted from Reference 20 summarizes work by the NASA Forensics Team. The analysis of the slag deposited on the inside of RCC Panel 8 shows that cerachrome and Inconel were deposited first in the slag layer. Deposition of aluminum occurred last. This is consistent with the sequence of thermal damage seen in the MADS/OEX data and is additional proof that the damage moved from the RCC -> aft. There were large amounts of melted cerachrome in the slag, consistent with prolonged presence of superheated air, since the melting point of cerachrome is in excess of 3200 °F. The presence of Inconel in the slag proves there was hot gas impingement on the RCC spanner bars, insulation foil and RCC panel fittings made of this material.

The absence of significant amounts of A286 stainless steel in the slag (Reference 20) suggests that the breach location was not close to these fittings. As shown by the figure, the deposition of Inconel spheroids and the

cerachrome tears and globules suggests a “splashing” effect of the flow entering from a hole below the apex of the RCC Panel 8. As discussed above, some of the flow exited out of the vent at the top, rear of RCC Panel 8 and some came out in a “sneak flow” in the slot in RCC Panel 8 outboard and eroded the carrier panel tiles below RCC Panel 9. In addition, the slag on the vertical surfaces of the internal LESS hardware was generally on outboard surfaces of the hardware inboard of Panel 8 and on the inboard surfaces of the hardware outboard of Panel 8.

Finally, it is noted in Reference 13 that all other recovered RCC panels on both wings have a generally uniform and thin slag layer. All analyzed slag layers show a uniform mix of aluminum, Inconel and cerachrome suggesting short exposure to superheated air and uniform melting of WLESS components.

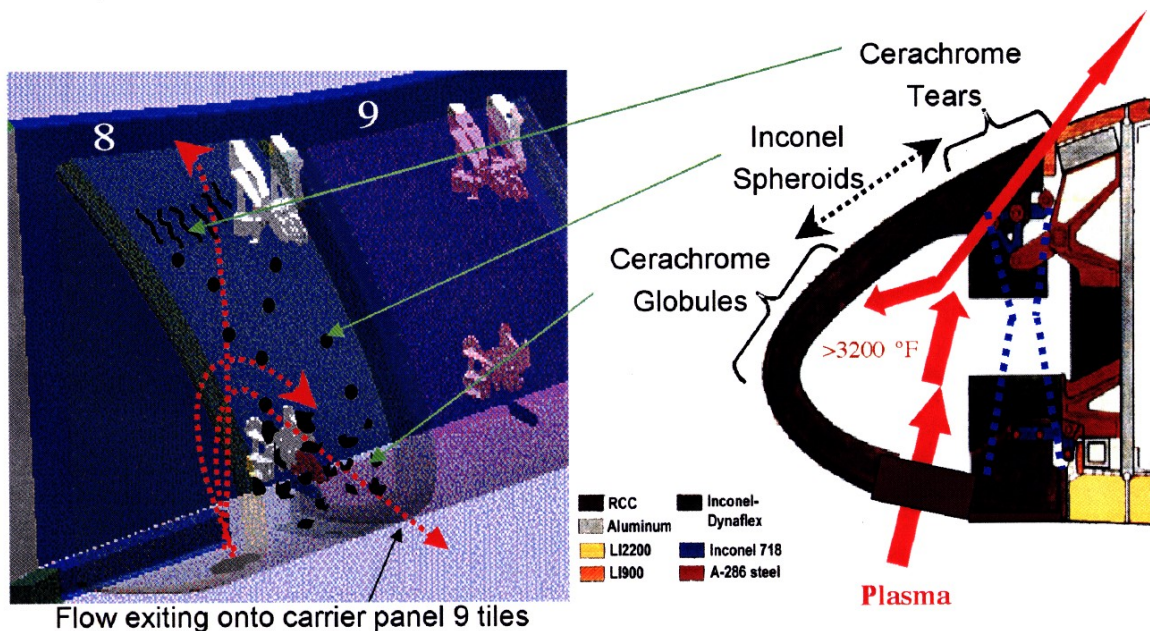


Figure 34: Wing Leading Edge Chemical Analysis of Panel 8 (Reference 20).

Recovered Tiles

Figures 35 and 36 show photographs of recovered tiles affixed to a 110 percent scale drawing of the left wing tile field. Here, a key of circular dots was used: Red means a tile is not in its final location, blue means a tile is in its final location and has been positively identified. Yellow means the tile failed at the densified layer, near the bond line and green means the tile failed owing to internal heating. In this case the Koropon/SIP failed or the Strain Insulation Pad (SIP) failed due to overheating. Koropon is the primer coating the aluminum skin.

There is a distinct pattern of RCG coated tiles, in the general X-direction downstream of Panels 8 and 9, outboard of the wheel well where the tiles appear to have little of the dark metal deposit (aluminum - rich) generally seen on the recovered tiles. These normal-appearing tiles all have been identified to have failure at the tile/Koropon bond line and departed from the wing surface prior to a major outflow of molten aluminum. This is indicative of extreme heat, inside the wing behind Panel 8. It then seems probable from this observation that the breach in the wing spar occurred at the Panel 8 location, and this is consistent with the observations discussed above. Ballistic analyses of the trajectories and the geographic location of the recovered tiles (both those detached owing to bond failure and those that did not) suggest they came off from about 100 nautical miles west of their recovery location in Texas.



Figure 35: Overview of Tile Table. Left Wing, Lower Surface Tiles.



Figure 36: View of Tile Table from RCC Panel 8/9 Area.

CFD and Engineering Simulations of Flow into Breach Through the RCC

The Columbia accident stimulated an extra ordinary effort by a national team led by NASA JSC (J. Caram {overall lead}, S. Fitzgerald {internal flow} and C. Campbell {external, damaged edge flow}) to understand the flow into the breach in the Columbia's RCC WLESS. This is a very difficult undertaking owing to the complex geometry inside the wing cavity and the lack of knowledge of the damage location as well as its shape and size. Such a complex analysis has never been done, and thus the team was truly "cutting new ground."

Initial study by Fitzgerald and his colleagues assumed that the external shock layer would provide a "plenum" of hot gas and that a jet (similar to those for nozzle flows) would enter the WLESS cavity, essentially normal to the locale of the hole. Early studies of localized heating from the jets and the resultant damage to the wing interior insulation were conducted. This work was of great help in understanding plume properties and developing tools.

P. Gnoffo (NASA Langley) and his colleagues (Reference 18), were the first to study the flow through a hole in an RCC panel using real-gas CFD with the LAURA code. The beginning point for this study was the external flow depicted in Figure 19. Gridding for a two-inch diameter hole in an RCC panel was introduced and flow studied for a simplified case with a hollow LESS cavity at a constant, rarefied pressure. This seminal work showed that the momentum of the external flows drives the jet in an outboard direction, "hugging" along the inside of the RCC. Subsequent work using LAURA for larger holes, up to 10 inches in diameter, demonstrated that more of the high enthalpy gas from the external shock layer is ingested as the hole diameter is enlarged. Additionally,

this work also demonstrated that: (a) an imbedded shock forms on the windward lip of the hole where extremely high temperatures (3,000 °K or 4,850 °F) are generated, assuming a fully catalytic materials response and (b) that the local inviscid shock layer flow over the wing is essentially unchanged as a result of the presence of the hole.

Subsequently, Boeing Huntington Beach (BHB) personnel (Reference 21) carried out internal CFD coupled to the external flow solution by Gnoffo, et. al., for a 6 inch hole in RCC Panel 7 where the 7/8 spanner and its insulation (“ earmuff”) were not modeled. These results gave lip-heating rates similar to the LAURA solutions. Further, they showed that the plume strikes the outboard RCC Panel 7 rib at a near normal angle of incidence, creating very high local convective heating rates.

The external flow solution by Gnoffo discussed above (Figure 19) was used by the Boeing Rocket Propulsion

and Power Group as a starting point for a CFD study (Reference 22) of the internal flow created by a 10 inch hole in RCC Panel 8. Their work utilized the ICAT CFD Code running equilibrium air and assumed fully laminar flow. The ICAT code was validated for this application through code-to-code (LAURA and a USA Code) comparison of predicted heat fluxes to a sphere in Mach 18 flow at an altitude of 165,000 ft. The calculation assumed constant boundary conditions into cavity dump regions of 0.087 psia (600 Pa).

Figure 37 depicts a view of the CFD results (Reference 22) from the front of the leading edge with the acreage of the panels rendered transparent. The hole in RCC Panel 8 is outlined on the lower left corner of the figure. Streamlines are color coded by Mach number and pressures on the earmuff and spar insulation “hot tub” are displayed by the color-coding shown in the figure. As can be seen, the subsonic flow is complex and the jet creates a significant high-pressure zone on the RCC 8/9 earmuff.

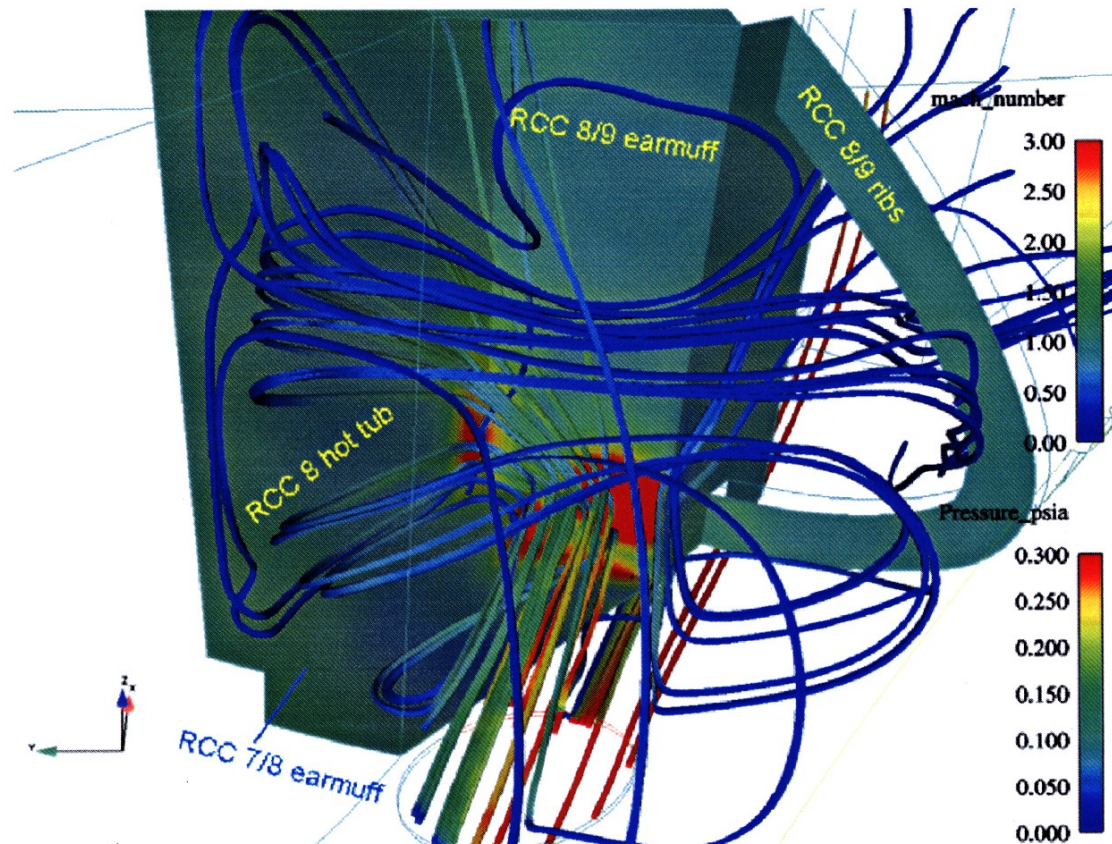


Figure 37: Results Adopted From Reference 22, Showing Streamlines From a 10” Diameter Hole in RCC Panel 8 (the Hole is Shown at the Lower Left). Acreage of RCC is Rendered Transparent. View is From Front of the RCC WLESS. Flight Conditions are Mach: 24.9, Altitude: 243 k ft, as in Figure 19. Pressure of 0.30 psia is Equal to 43.2 psf.

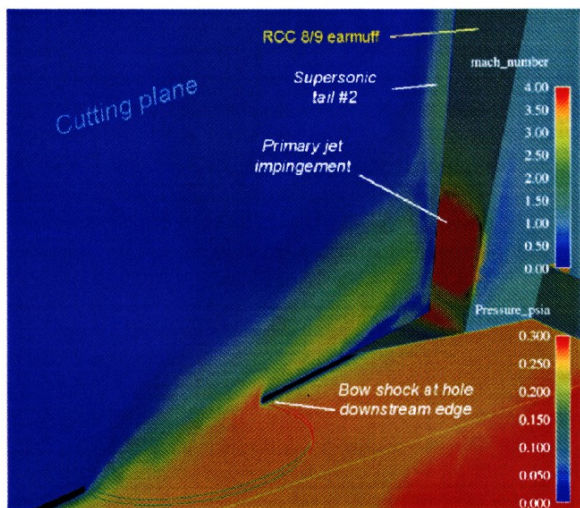


Figure 38 (a): CFD Predictions for Wall Static Pressure and Mach Number for a 10" Hole in RCC Panel 8, Corresponding to Solution in Figure 37. Static Pressure is Color Coded on Walls and Mach Number Distribution is Shown on the Cutting Plane.

Figure 38 (a) from the Boeing Propulsion and Power group depicts the static pressure on the WLESS internal walls and the Mach number on the cutting plane, which passes through the 10 inch diameter hole. The results indicate that all of the external boundary layer and some of the local inviscid (freestream) flow is ingested into the WLESS channel. The primary jet strikes the earmuff at a near-normal incidence (80°). Its stagnation pressure exceeds the freestream-shock pressure because of a precompression by the oblique vehicle shock.

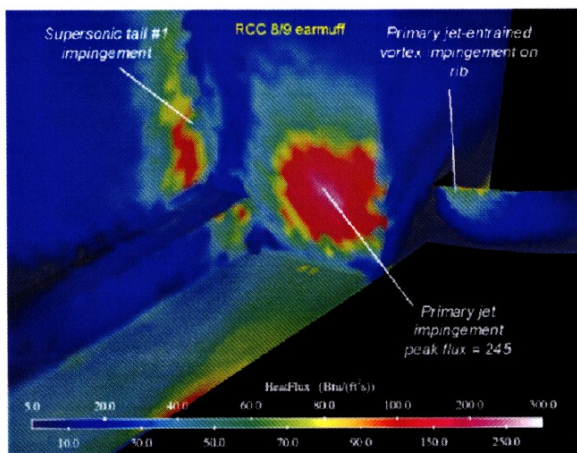


Figure 38 (b): CFD Predictions for Convective Heat Flux on Hot Tubs, Earmuff and Rib for a 10" Hole in RCC Panel 8, Corresponding to the Solution in Figure 37.

Figure 38 (b) shows CFD predictions for convective heat transfer to the spar insulation (hot tub), spanner insulation (earmuff) and the RCC outboard rib corresponding to the solutions shown in Figures 37 and 38 (a). The heat fluxes on the earmuff at the center of the jet impingement are significantly higher than that of an undamaged wing, immediately upstream of the breach in Panel 8 with a finite catalytic wall (Reference 18) (300 vs. 27.3 Btu/ft²s).

In summary, this seminal work has shown that the flow in holes from 2 -> 10 inches in diameter allow superheated air jets to impinge on the inner surfaces of the WLESS creating complex internal flows with significant local heating rates significantly higher than those which occur on the exterior of an undamaged wing leading edge during the normal functioning of the Shuttle.

The results from the BHB study (Reference 21) were available when the CAIB requested arc jet simulations to demonstrate that super heated airflows inside the WLESS could cause sharpening of the RCC seen in the Columbia debris. They were used to define test conditions for arc jet simulations of RCC sharpening to be discussed below.

Arc Jet Simulations of Super Heated Flow Causing Ablation and "Sharpening" of RCC

Arc jet testing discussed by Curry, et. al., in 2000 (Reference 5) has shown that superheated air can cause "sharpening" of RCC when the SiC coating has been removed, the surface temperature of the undamaged SiC is at 2800 °F or greater and the pressure is 30 psf or greater. This testing was done on small circular holes in RCC samples, caused by simulated micrometeorite damage. Figure 39 shows the arc jet test set-up used in this testing.

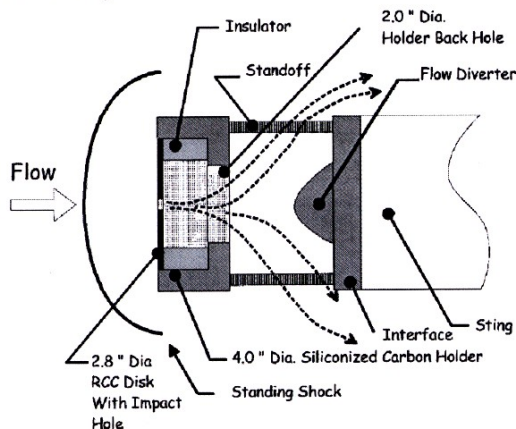


Figure 39: Arc Jet Test Set-up for Micrometeorite Testing of RCC (Reference 5).

Figure 40 displays photographs of the test article number 1159 pre and post arc jet test. Test conditions resulted in a surface temperature and pressure on test article number 1159 of 2500 °F and 50 psf, respectively. The exposure was for 450 seconds. Figures 40 c) -> 40 e) show that in this case, the hole growth grew by oxidation of the exposed carbon-carbon substrate. The oblique view in Figure 40 e) illustrates the “dishing out” of the carbon sandwiched between the SiC front and back coating. For these test conditions, Curry, et. al., did not expect hole growth owing to loss of the SiC coating because of its stability up to temperatures in the range of 2800-3000 ° F and this was confirmed by the tests.

Figure 41 displays photographs of test article number 1151, pre and post test. The temperature of exposed carbon at the SiC edge reached 3,250 °F +. For this test condition (2800 °F and 100 psf), there was significant front face SiC coating erosion as shown in Figures 41 c) and d). Curry, et. al., noted that in general, the front face of the damaged region grew faster than the backside of the specimen, resulting in a conical, or “sharpened shape,” typical of all of their testing at a nominal temperature of 2800 °F.

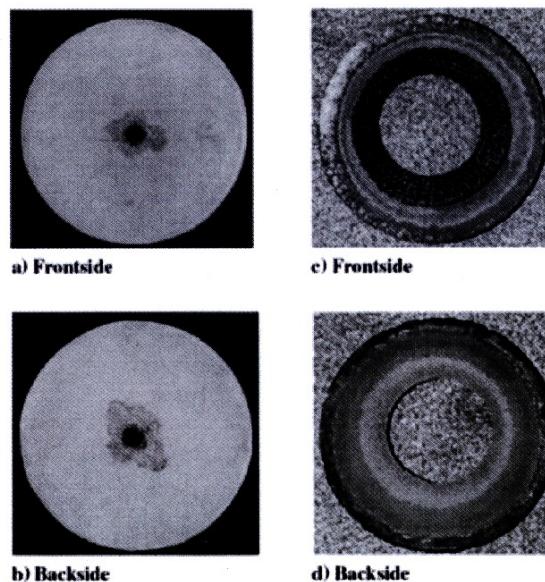


Figure 41: NASA/JSC Model Number 1151, Pre and Post Arc Jet Exposure at 2800 °F and 100 psf, 450 Second Exposure. (Reference 5).

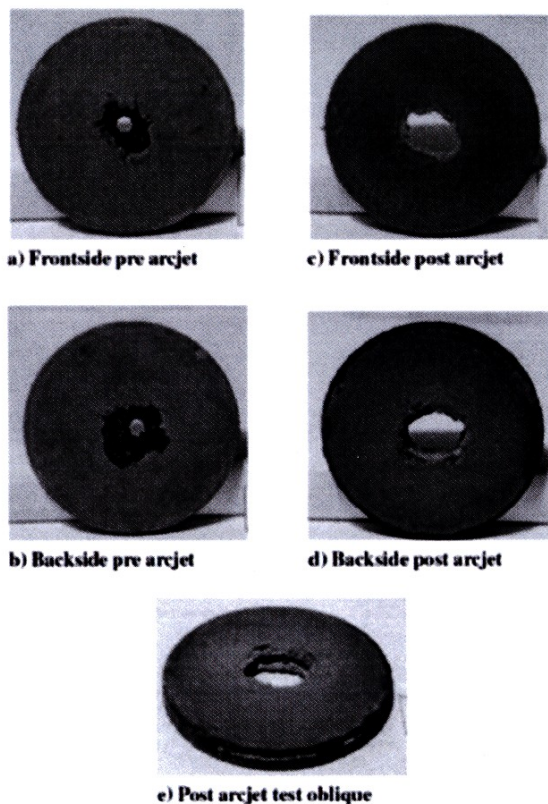


Figure 40: NASA/JSC Model Number 1159, Pre and Post Arc Jet Exposure at 2500 °F and 50 psf, 400 Second Exposure. (Reference 5).

It can be concluded from these tests that the dominant mechanism for the ablation of RCC with the coating removed is diffusion-controlled oxidation. At the higher temperatures, SiC coating loss is expected. This result, which causes “knife edging” for a circular hole suggests that if RCC was damaged in a linear fashion, one would see formation of knife-edges in superheated air heating environments existing for hundreds of seconds in conditions like those in the arc jet tests discussed in Reference 5. This observation was the basis for the discussion of the “knife edging” seen in the RCC Panel 8/9 debris from Columbia.

In order to further determine if knife edging would occur on coated RCC due to flow inside the wing from a hole in Panel 8/9, additional arc jet tests (Reference 6) were performed in the JSC facility at the request of the CAIB. Two test articles were designed, built and tested. Test conditions were defined to simulate the flow into the wing based on the Boeing Huntington Beach CFD results previously discussed.

The first test, with two parallel plates shown in Figure 42 with flow impinging at 70 degrees to the flat face was intended to simulate the flow inside the wing impinging on RCC ribs. The results of the test on the parallel plates was inconclusive, because the surface temperatures attainable, without damaging the model holder, were not high enough to cause ablation of the SiC coating.

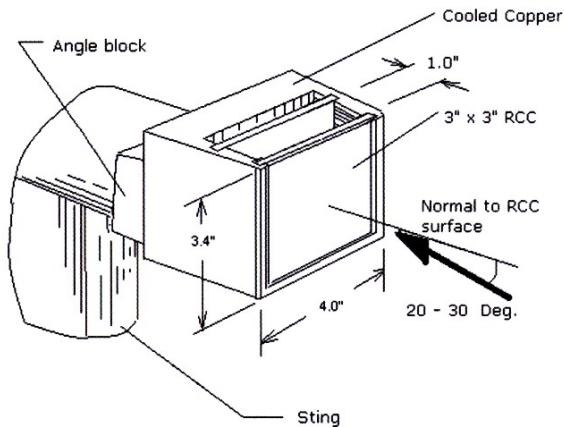


Figure 42: NASA/JSC Arc Jet Test Set-up for Linear Knife-edge Tests at Large Angle of Incidence (70°). Test to Simulate Flow Impingement on RCC Ribs.

The second test article, shown in Figure 43, was intended to simulate flow on the windward lip of a hole in Panel 8. This test, with a flow angle on the single plate at 20 degrees incidence showed that knife edging would occur when the temperature on the coated leading edge of the plate was above 3250 °F. Table 3 specifies the test conditions thought to simulate the enthalpy and impact pressure present in the damaged wing during Columbia's entry on STS 107.

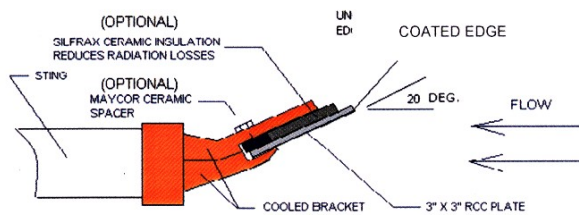


Figure 43: NASA/JSC Arc Jet Test Set-up for Simulation of RCC Knife-edge Erosion at Low Angle of Incidence (20°). Test Intended to Simulate Flow on Lip of Hole in RCC Panel.

Condition	Bulk Enthalpy (BTU/lbm)	Impact Pressure (psf)	Duration (sec)
1	11,200	75	350
2	10,800	129	173

Table 3: Operating Conditions for Tests Shown in Figure 44.

Figure 44 (a) is a pre-test photograph of the test article. Note that the coated edge of RCC is facing the flow for both the RCC sample and the RCC closeout pieces placed on either side.

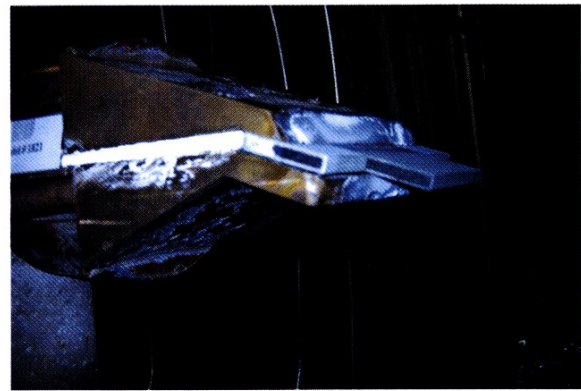


Figure 44 (a): Pre-test Photograph. Angle of Incidence: 20°, Coated Edge Facing Flow.



Figure 44 (b): Post-test Photograph Showing Knife-edges in Both RCC Test Article and Closeout.



Figure 44 (c): Close Up, Post-test Photograph Showing Knife-edges in the RCC Closeout.

Figure 44 (b) is the corresponding post-test photograph of the test article. Here, erosion of the SiC coating is apparent, as is the formation of a knife-edge on the primary RCC sample, where the highest temperatures occurred. The edge temperature was in excess of 3200 °F or greater as shown by the failure of the SiC coating. Furthermore, as shown in Figure 44 (c) knife-edges also formed in the SiC coated RCC closeouts where flow from the primary RCC sample was impinging.

Tests like those just described were also performed using a test article with an uncoated RCC edge. Similar knife-edges were formed as a result of exposure to the superheated air stream, as expected.

The arc jet tests performed for the CAIB investigation and those previously performed by Curry, et. al. can be used to understand the process by which knife-edges were formed on the RCC components inside Columbia's damaged wing during entry.

If the heat transfer from the superheated airflows creates temperatures in excess of 3200 °F and impact pressures of greater than about 30 psf for extended times, the SiC coating will fail. The SiC coating on the RCC is stable to about 3200 °F, at which temperature it oxidizes, forming liquid silica glass, which either flows off the carbon surface or is evaporated as the temperature goes even higher. The same heating environment that heats the silicon carbide to 3200 °F will heat the exposed carbon to much higher temperatures because the exothermic oxidation of the carbon increases the energy at the surface. Once the carbon has been exposed by removal of the coating, the ablation process becomes more intense because the temperature at the interface between the coating and the carbon substrate gets higher and the SiC removal rate increases.

When the flow is at an angle to an edge (Figures 42 and 43), the heat transfer and mass transfer of oxygen will be higher on the windward side than the leeward side, so the SiC will be removed faster on the windward side. The heat transfer and diffusion of oxygen to the surface is the highest at the exposed sharp edge. As the gas flows downstream along the surface of the plate, the boundary layer becomes thicker and the heat flux and oxygen diffusion rate to the surface lowers. The amount of carbon that burns off decreases, because it is controlled by the rate of oxygen diffusion to the surface. As long as the temperature at the interface of the carbon and the silicon carbide coating is above the oxidation temperature of the silicon carbide this process will continue. When the temperature drops below that value the silicon carbide remains in place and protects the carbon. That is why, in the earlier tests by Curry, et. al., (Figure 41) and in the test results shown in Figure 44, the surface of the model facing the flow shows the knife edging and the back of

the test article does not. The temperature on the back does not become high enough to oxidize the silicon carbide. At low heat flux the broken or penetrated edge of the RCC will experience ablation/recession of the carbon between the two silicon carbide coated surfaces causing a cavity. The silicon carbide will not recede because it never reaches its oxidation temperature (3200 °F).

It is probable that some broken edges of internal RCC were formed by the foam impact. In either case for RCC, coated or uncoated, knife-edges would be formed, provided that high temperatures and pressures of the type described above are present for extended periods. It is also possible that the SiC coating was damaged on relatively large, broad areas of the internal RCC surfaces due to the impact of fractured RCC and foam debris ejected from the back surface of the initial foam impact hole. This could have caused significant micro-cracking of the SiC coating on the surfaces facing the rear of the impact hole, i.e., the flow-facing, front side of the internal RCC pieces. In this case, surface recession would have occurred over relatively large areas of the damaged flow facing surfaces as the oxygen reached the carbon through the cracks in the SiC coating. This would produce very thin RCC panels with significant carbon removal on the front side and practically no damage to the rear side as is illustrated in Figures 28 and 29.

The exact configuration of the final knife-edge is highly dependent on the exposure time, heat flux, flow angle and initial condition of the edge. If the heat flux is high enough, the longer the exposure, the sharper the knife-edge is likely to get. If the edge is initially broken at an angle to the surface of the knife-edge, it is likely to be sharper. Inspection of the RCC ribs illustrated in Figures 28 and 29 show very sharp edges that indicate a long exposure to high heating rates. This indicates that this debris was exposed to high heating early during Columbia's final atmospheric entry lasting until break-up.

Summary

The authors have analyzed available information to confirm or refute Admiral Gehman's aforementioned hypothesis made in early February: During launch, an ET foam strike compromised the RCC left wing of Columbia. The breach was present at the Entry Interface (EI) and during entry severe internal heating occurred, the wing structure failed and this led to the tragic loss of Columbia and the STS 107 crew. As assigned, the focus of this analysis was on the TPS.

The vehicle re-entry environment of the Space Shuttle for a normal (undamaged vehicle) was reviewed in order to help the reader understand the need for TPS. A synopsis of the design and function of the Shuttle TPS was also

presented so the reader could understand how it performs during normal entry (successfully over one hundred missions).

Supporting evidence for the strike of ET foam and damage it may have inflicted is the subject of study by others. Analysis of launch films and video, together with CFD study of the transport of the foam trajectory, conclude that the area struck was in the area of the lower RCC panels from 5-8. Tests at Southwest Research Institute and physics-based models show that foam impacts can cause severe damage/cracking to RCC panels and T-Seals, physical displacement of parts and the formation of large holes (16 by 16 inches).

The analysis herein started with an assumption that the RCC compromise was in the areas of RCC Panels 5-8. Increasingly, the information developed strongly suggested that the breach was in the lower part of Panel 8, and that part of the upper T-seal between Panels 8 and 9 was missing or severely displaced at entry interface.

MADS/OEX data from a thermocouple mounted behind the leading edge wing spar, behind Panel 9 recorded out-of-family temperature increases during ascent, after the foam strike at 82 seconds into the launch. Analysis by NASA suggests that a hole in Panel 8, of 6 -> 10 inches in diameter could account for this temperature rise. Since the temperature rise is small, this information by itself is insufficient to confirm the hypothesis. However, with the preponderance of other information available, it does strongly suggest that the breach was in place at the entry interface, which occurred 16 days later.

MADS/OEX data from four sensors in the span of time from GMT 13:47:00 to 13:50:00 show the progression of damage is from the RCC toward the aft of the vehicle. The first indication is from a strain gage mounted on the spar, behind Panel 9. Its signal was interpreted to be caused by the RCC cavity being pressurized and building up thermal stress in the wing leading edge. Shortly thereafter, a thermocouple in the RCC mounting clevis, inside the wing leading edge at the Panel 9/10 area recorded a slight temperature increase. Then a thermocouple on the back of the spar behind RCC Panel 9 also displayed a temperature rise. Finally, in this span of time, the left OMS Pod thermocouple showed an initial below nominal trend. Wind tunnel data showed that this was likely caused by a flow field disturbance in the RCC Panel 5-10 region.

The interval from 13:52:00 -> 14:00:00 includes three key observations, which correlate with the hypothesis. First, the thermocouple on the back of the spar behind Panel 9 showed an abrupt increase at 13:52:19 (EI + 487 seconds) interpreted to be caused by superheated air penetrating the spar. Increasing heating on the OMS Pod correlates with

debris leaving Columbia in events 1 - 13 occurring in the two minute time frame from 13:53:29 -- 13:55:29. At 13:57:14, a photograph taken from the Starfire facility at Kirtland Air Force Base shows left wing damage that is consistent with the hypothesis. Compelling evidence to support the hypothesis comes from the debris from Columbia and its forensic analysis. Study of the recovered debris revealed significant damage in the RCC Panel 8/9 area. This included significant erosion, or "sharpening" of the very durable RCC and melting of metal fixtures and insulation, internal to the WLESS. Significant RCC erosion and melting of LESS RCC mounting hardware is observed only in the Panel 8/9 area of the left wing. This debris evidence is believed to have occurred during exposure to a superheated flow environment lasting for hundreds of seconds. Arc jet simulations of RCC in such a superheated air stream support this conclusion. Flow out of a slot in the juncture between RCC Panels 8 and 9 caused severe erosion and flow patterning on the carrier panels below RCC Panel 9. Streamlines from CFD solutions indicate that flow from this juncture washed over the thermocouple in the lower tile field, behind Panel 9. This thermocouple registered off-nominal heating during the STS 107 entry correlating well with the hypothesis.

Chemical analysis of "slag" on the debris showed that the composition of deposits closest (earliest) to the interior of the RCC upper Panel 8 correlates with the metal spanner bars and mounting hardware and cerchrome insulation. Outer (later) portions correspond to the aluminum deposition. This sequencing also correlates with the hypothesis.

Finally, analysis by NASA using both CFD and engineering analysis tools show a strong correlation of the observations (ascent heating, entry heating, timing for spar burn-through and OMS pod off-nominal high and low temperature) to those that would occur if a 6 -> 10 inch diameter hole existed in the lower section of RCC Panel 8 at entry interface.

Conclusion

Based on the information and analysis presented above as well as combined experience in the fields of aerothermodynamics, TPS, entry technology development and ballistic missile re-entry design and test, the authors believe that the hypothesis by the CAIB chair actually occurred.

Based on data and analysis, the general hypothesis that the accident was caused by a compromise to the Left Wing RCC from the ET foam strike has been narrowed considerably. The authors believe it is quite likely that the breach caused by the foam strike was equivalent to a hole

of at least 6 → 10 inches in diameter in RCC Panel 8. Further, the upper part of the T-Seal between Panels 8 and 9 was missing or severely displaced. The damage existed at Entry Interface.

The authors assign a probability of 95 percent that the hypothesis above occurred, based on the preponderance of information available with 100 percent being absolute certainty.

Finally, the authors also point out that there has been an unwarranted tendency to “fault” the TPS for the Columbia accident. Clearly, the root cause of this accident is the ET foam strike. The design and implementation of the Shuttle TPS was and is a brilliant accomplishment, which for the first time enabled a reusable vehicle to undergo hypervelocity, atmospheric flight. Recommendations made by others for increasing the safety and reliability of the existing TPS may make the system even better for the Shuttle and future reusable vehicles. However, methods to decrease or eliminate impacts to the TPS by large or heavy objects, will be the most significant advances to the overall Shuttle safety and reliability.

Acknowledgements

We respectfully acknowledge the achievement of the thousands of NASA personnel and NASA contractors who developed the Space Shuttle during the late 1970 – 1981 time frame.

We acknowledge the tireless efforts by NASA and contractor personnel who have contributed to understanding what happened to cause the tragic loss of the STS 107 crew and Columbia. Much of the work herein is the result of their labor. Special acknowledgement is made for those who have worked so hard at KSC to reconstruct the debris. These include, Julie Kramer White, Mike Gordon, Tom Roberts, Lisa Huddleston, Janet Ruberto, Jim Meyers, Lyle Davis and Ann Micklos. We acknowledge the excellent support of Liz Fountain, Mike Conely and Tony Griffith of the JSC Columbia Task Force Team. Some of the charts, used herein, are adopted from NASA JSC/Boeing briefings by Phil Glynn/Mark Hasselbeck/Gene Grush/Steve Stitch, and we acknowledge excellent collaborations with them. We acknowledge the support by S. Bouslog, Lockheed Martin, in defining arc jet test conditions and the help of Jim Milhoan in the design of the arc jet tests. The technical support of J. Williams, J. Grinstead, Mark Tanner, Greg Kovacs and L. Chu-Thielbar is gratefully acknowledged. We appreciate Dr. J. Hallock’s review of this appendix and Marla Arcadi’s help in preparing the manuscript.

Finally, we acknowledge the very fruitful collaborations

at the KSC debris site with the Boeing Debris Analysis Team of Larry Korb, Mike Ehret, and Don Hendrix. James Reuther’s expertise in fluid flows in analyzing RCC Panel 8/9 debris at KSC was very helpful as well.

References

1. G. Burns, et. al., NASA Final Report, “Image Analysis” of ET foam Strike to Columbia/STS 107, Month 2003.
2. R. Gomez, et. al., NASA Final Report, “Transport CFD Analysis of Foam Strike on STS 107,” Month 2003.
3. G. S. Hubbard and P. Wilde, “ET Impact Testing and Analysis,” Appendix,_CAIB Final Report, Month 2003.
4. R. B. Darling, “Qualification and Interpretation of Sensor Data from STS 107,” Appendix_CAIB Final Report, June 2003.
5. D. M. Curry, V.T. Pham, I. Norman, and D.C. Chao, “Oxidation of Hypervelocity Impacted Reinforced Carbon-Carbon,” NASA/TP-2000-209760, March 2000.
6. A. Rodriguez, Section 6.10, Reference 7.
7. P.Madera, S. Labbe, J. Caram, C. Madden and M. Dunham (Principal Authors), et. al., “Aero/Aerothermal/Thermal/Structures Team Final Report in Support of the Columbia Accident Investigation,” NSTS-37398, July 2003.
8. H. J. Allen and J. A. Eggers, “A Study of the Motion and Aerodynamic Heating of Missiles Entering the Earth’s Atmosphere at High Supersonic Speeds,” NACA RM-A53D28, August 1953.
9. D. Prabhu, M. Wright, J. Marvin, J. Brown, and E. Venkatapathy, “X-33 Aerothermal Design Environment Predictions: Verification and Validation,” AIAA Paper 2000-2686, June 2000.
10. P. A. Gnoffo, K. J. Weilmuenster, S. J. Alter, “Multiblock Analysis for Shuttle Orbiter Re-entry Heating from Mach 24 to Mach 12,” *Journal of Spacecraft and Rockets*, Vol. 31, No. 3, May-June 1994, pp 367 – 377.
11. T. J. Kowal and D. Curry, “Orbiter Thermal Protection System (TPS) Overview,” 2/10/03.
12. A. Rodriguez and C. Madden, Section 6.1, Reference 7.
13. CAIB/NAIT, “Columbia Working Scenario Final Report,” NSTS-60502, July 2003.

14. T. J. Horvath and N.R. Mirski, Section 5.2, Reference 7.

15. D. L. Potter, "Columbia Signal Attenuation Modeling PIRATE Scoping Study," Private Communication.

16. J. Caram, Section 5.2, Reference 7.

17. S. Widnall, CAIB Report Section on Aerothermodynamics, August 2003.

18. P. A. Gnoffo, S. J. Alter, and R. A. Thompson, Section 5.2, Reference 7.

19. C Madden, Section 6.2, Reference 7.

20. J. Kramer White, M. Eharet, L. Korb, D. Hendirx, et. al., "Hardware Forensics Team Final Report," NSTS-37385, June 12, 2003; and J. Kramer White, "Failure Analysis Final Report to OVWEG in Support of Columbia Accident Investigations," June 23, 2003.

21. K. Rajagopal, et. al. (Boeing Huntington Beach), Section 5.3, Reference 7.

22. S. Halloran and S. Barson, et. al. (Boeing Propulsion and Power), Section 5.3, Reference 7.

THIS PAGE INTENTIONALLY LEFT BLANK